MOLECULAR AND CELLULAR BIOLOGY, Feb. 2011, p. 388–403 Vol. 31, No. 3
0270-7306/11/$12.00 doi:10.1128/MCB.00969-10

p21-Activated Kinases 1 and 3 Control Brain Size through Coordinating Neuronal Complexity and Synaptic Properties▽

Wayne Huang,[1,3]† Zikai Zhou,[1,3]† Suhail Asrar,[1,3] Mark Henkelman,[2,4] Wei Xie,[5] and Zhengping Jia[1,3]*

Neurosciences & Mental Health[1] and Mouse Imaging Centre (MICe),[2] The Hospital for Sick Children, 555 University Ave., Toronto, Ontario, Canada M5G 1X8; Department of Physiology[3] and Department of Medical Biophysics,[4] University of Toronto, Toronto, Canada; and Key Laboratory of Developmental Genes and Human Disease, Ministry of Education, Institute of Life Sciences, Southeast University, 2 Sipailou Road, Nanjing 210096, China[5]

Received 18 August 2010/Returned for modification 21 September 2010/Accepted 12 November 2010

The molecular mechanisms that coordinate postnatal brain enlargement, synaptic properties, and cognition remain an enigma. Here, we demonstrate that neuronal complexity controlled by p21-activated kinases (PAKs) is a key determinant for postnatal brain enlargement and synaptic properties. We showed that double-knockout (DK) mice lacking both PAK1 and PAK3 were born healthy, with normal brain size and structure, but severely impaired in postnatal brain growth, resulting in a dramatic reduction in brain volume. Remarkably, the reduced brain size was accompanied by minimal changes in total cell count, due to a significant increase in cell density. However, the DK neurons have smaller soma, markedly simplified dendritic arbors/axons, and reduced synapse density. Surprisingly, the DK mice had elevated basal synaptic responses due to enhanced individual synaptic potency but were severely impaired in bidirectional synaptic plasticity. The actions of PAK1 and PAK3 are possibly mediated by cofilin-dependent actin regulation, because the activity of cofilin and the properties of actin filaments were altered in the DK mice. These results reveal an essential *in vivo* role of PAK1 and PAK3 in coordinating neuronal complexity and synaptic properties and highlight the critical importance of dendrite/axon growth in dictating postnatal brain growth and attainment of normal brain size and function.

Attainment of normal brain volume is critical for proper brain function. Thus, reduced brain size, characteristic of a class of neurodevelopmental disorders called microcephaly and its related cortical malformations, is usually accompanied by impaired intellectual abilities and other neurological defects. Microcephaly can be primary or secondary, depending on whether the defect occurs before or after birth (40, 41, 58). Numerous studies have shown that the generation of neurons (or neurogenesis) is the main determinant of embryonic brain growth (8, 16, 18, 21, 45, 52). However, the mammalian brain continues to undergo rapid growth even after birth, and because neurogenesis is already completed, it is assumed that the growth of individual neurons is a key driving force for this postnatal brain enlargement. Surprisingly, the experimental evidence to support this notion is limited. In addition, the relationship between reduced brain size and cognitive/behavioral deficits remains unclear, because most of the mouse models with primary microcephaly are either lethal or grossly altered in whole-body growth or brain structure (12, 18, 21, 27, 52), thus preventing meaningful functional studies in these mice.

p21-activated kinases (PAKs) are a family of serine/threonine proteins that can be activated by multiple signaling molecules, particularly the Rho family small GTPases, the central regulators of the cytoskeletal structure (5, 11, 60). Among the six known mammalian PAKs, the group I PAKs (PAK1 to -3) are most extensively studied for their *in vitro* functions, of which the regulation of cell motility, migration, morphology, and cytoskeleton reorganization is best known (5, 11, 31, 43, 60). Recent studies on neurons also indicate that PAKs are important for neurite outgrowth, neuronal migration, spine morphology, and synaptic and behavioral plasticity (9, 10, 13, 15, 17, 23–25, 29, 30, 36, 50, 59). However, despite these demonstrated *in vitro* functions, the *in vivo* roles of PAKs, particularly in mammalian brain development, remain elusive. Genetic deletions of individual PAKs in mice have thus far produced limited information, possibly due to functional redundancy among these molecules (2, 7, 32, 39, 42, 48). For example, knockout (KO) mice lacking either PAK1 or PAK3 exhibit no abnormalities in overall neuronal morphology and brain development (7, 39). However, it is known that mutations in the *PAK3* gene are linked to mental retardation characterized by secondary microcephaly in humans (3, 46), suggesting a critical role for PAKs in postnatal brain development and attainment of normal brain volume. The pathogenic mechanisms by which *PAK3* gene mutations cause this brain disorder remain unknown.

In this study, we provide genetic, morphological, electrophysiological, and behavioral evidence indicating that PAK1 and PAK3 control brain size through coordinating neuronal complexity and synaptic properties.

MATERIALS AND METHODS

PAK1/PAK3 DK mice. The generation of PAK1 and PAK3 single-knockout mice were described previously (7, 39). Heterozygous mice for both PAK1 and PAK3 ($PAK1^{+/-}$ $PAK3^{+/-}$) were interbred to generate PAK1/PAK3 double-

* Corresponding author. Mailing address: Neurosciences & Mental Health, The Hospital for Sick Children, 555 University Ave., Toronto, Ontario, Canada M5G 1X8. Phone: (416) 813-8713. Fax: (416) 813-7717. E-mail: zhengping.jia@sickkids.ca.
† These authors contributed equally.
▽ Published ahead of print on 29 November 2010.

knockout (DK) mice ($PAK1^{-/-}$ $PAK3^{-/-}$). For all the experiments reported here, the wild-type (WT) or heterozygous littermates ($PAK1^{+/+}$ $PAK3^{+/+}$ or $PAK1^{+/-}$ $PAK3^{+/-}$) were used as controls for the DK mice. Whenever possible, the experimenters were blind with respect to the genotype of the mice used.

MRI analysis. Detailed procedures and image analysis for magnetic resonance imaging (MRI) were described previously (19) and are briefly summarized below. Animals were anesthetized with ketamine via intraperitoneal injection. Thoracic cavities were opened, and the mice were perfused through the left ventricle with 30 ml of phosphate-buffered saline (PBS) (pH 7.4) at room temperature. This was followed by infusion with 30 ml of iced 4% paraformaldehyde in PBS. Following perfusion, the heads were removed along with skin, lower jaw, ears, and cartilaginous nose tip. The remaining skull structures containing the brain were allowed to postfix in 4% paraformaldehyde at 4°C for 12 h. The skulls were then transferred to 2 mM ProHance (Bracco Diagnostics Inc., Princeton, NJ) and 0.01% sodium azide in PBS solution and stored at 4°C until MRI. A multichannel 7.0-T MRI scanner (Varian Inc., Palo Alto, CA) with a 6-cm-inner-bore-diameter insert gradient set was used to acquire anatomical images of brains within skulls. Prior to imaging, the samples were removed from the contrast agent solution, blotted, and placed into 13-mm-diameter plastic tubes filled with a proton-free susceptibility-matching fluid (Fluorinert FC-77; 3M Corp., St. Paul, MN). Three custom-built, 14-mm-diameter solenoid coils with a length of 18.3 cm were used to image three brains in parallel. Parameters used in the scans were optimized for gray/white matter contrast: a T2-weighted, three-dimensional (3D) fast spin echo sequence, with repeat time equal to 325 ms and echo time equal to 32 ms and four repeated data acquisitions, field of view of 12 by 12 by 25 mm, and matrix size of 432 by 432 by 780, giving an image with 32-μm isotropic voxels, optimized for image-based registration. Total imaging time was 11.3 h when three brains were scanned simultaneously. Geometric distortion due to the position of the three coils inside the magnet was corrected using an MR calibration phantom. A series of image registration methods was used to bring 8 DK mice and 7 WT mice into alignment. The result of the registration process is to have all brains deformed into exact alignment with each other, to generate 1 atlas for WT and 1 for DK mice. Both these atlases were nonlinearly aligned to a 3D atlas of the mouse brain with 62 structures identified, enabling the absolute volume information to be obtained for these structures. Only structures greater than 3 mm^3 in volume were analyzed. All reported results were significant at a 0.1% false discovery rate.

Histology, immunohistochemistry, and electron microscopy. The procedures for histology, immunohistochemistry, and electron microscopy (EM) of fixed brain tissues were described previously (38). Images of the stained brain sections were collected on a Zeiss Mirax scan and Leica fluorescence stereomicroscope (low magnifications) or Nikon TE2000 and Zeiss confocal microscopes (high magnifications) and analyzed with Volocity 4.4 (PerkinElmer) or ImageJ software. Primary antibodies used for immunohistochemical analyses included anti-Tbr1 (Millipore), anti-Cux1 (Santa Cruz), anti-FluoroMyelin green (Invitrogen), anti-GluR1 (Chemico), antisynapsin (Santa Cruz), anti-MAP2 (Millipore), anti-phospho-neurofilament (pNF) (Sternberg Inc.), anticofilin (Cytoskeleton), and anti-*p*-cofilin (Santa Cruz). For the analysis of synapse density and size, a total of approximately 80 to 100 EM micrographs covering approximately 6,800 to 8,000 μm^2 from two animals per genotype were quantified using ImageJ software. For stereological cell counting, fixed brains were crystated into 40-μm sections across the forebrain, and sections were collected every 280 μm (1 in every 7 sections). To estimate the total cortical neurons, sections were floating stained with NeuroTrace 500/525 green fluorescent Nissl (Invitrogen), and the neuronal cell bodies were counted using the standard optical fractionator technique with the Nikon TE2000 histology microscope using Volocity 4.4 software. A 150- by 150-μm sample frame was used for counting. For the cortical region on each section, six randomly selected frames were counted: two from layers I to III, two from layers IV and V, and two from layer VI. Based on the cortical volume and the neuronal densities in a given section, the total amount of cortical neurons for that section was then estimated. The sum of neuronal count in all sections throughout the forebrain (multiplied by a correction factor of seven) provided an estimate of the total neurons in one half of the cortex. The same stereological method was used to estimate the number of hippocampal glia using hippocampal sections costained with DAPI (4′,6-diamidino-2-phenylindole) and glial fibrillary acidic protein (GFAP). The total glia in the hippocampus was estimated by multiplying the glial densities in the CA1 region by the corresponding hippocampal volume.

Golgi impregnation. The general procedure for Golgi staining was described previously (38) but modified according to the instructions of the manufacturer of the staining kit (FD NeuroTechnologies, Germantown, MD). Briefly, whole brains were treated for silver impregnation for 1 week, cryoprotected for 48 h, and sectioned at 100 μm (for spine analysis) and 200 μm (for dendrite analysis) on a cryostat. After sectioning and mounting on gelatin-coated slides, sections were developed, clarified, and mounted in resinous medium (Permount mounting medium). The entire-section images were captured using a Zeiss Mirax scan. Individual neurons were visualized using a Nikon TE2000 histology microscope. Dendritic spines were analyzed using Volocity software (Improvision).

Western blot analysis. Whole-brain lysates were used to estimate the total amount and phosphorylation levels of various proteins. For each experiment, protein samples (10 μg of total proteins) of each genotype were loaded on SDS gel (samples from the DK mice were always loaded side by side with those from their wild-type littermates for better comparison) and examined by Western blot analysis. The amount of each protein detected by the enhanced chemiluminescence (Amersham Biosciences, Piscataway, NJ) method was estimated by scanning the optical density of the blot. The primary antibodies used in Western blot analysis included anti-*p*-cofilin (Santa Cruz), anti-pCREB (Santa Cruz), anti-pP44/42 (Cell Signaling Technology), anti-pMLCK (Santa Cruz), anti-MAP2 (Upstate Biotechnology), anti-PAK1 (Santa Cruz), anti-PAK3 (Santa Cruz), anticofilin (Cytoskeleton), anti-CREB (Upstate Biotechnology), anti-ROCK1/2 (Santa Cruz Biotechnology), anti-P44/42 (Cell Signaling Technology), anti-MLCK (Santa Cruz), anti-GluR2/3 (Chemicon), antisynapsin (Santa Cruz), and antitubulin (Cytoskeleton).

Electrophysiology. The detailed procedures and analysis for hippocampal slice recordings were described previously (38, 39). The extracellular artificial cerebrospinal fluid (ACSF) contained 120 mM NaCl, 3.0 mM KCl, 1.2 mM $MgSO_4$, 1.0 mM NaH_2PO_4, 26 mM $NaHCO_3$, 2.0 mM $CaCl_2$, and 11 mM D-glucose. For whole-cell recordings, hippocampal CA1 neurons were visualized using an infrared differential interference contrast microscope (Zeiss Axioscope). The intracellular solution contained 130 mM $CsMeSO_4$, 5 mM NaCl, 1 mM $MgCl_2$, 0.05 mM EGTA, 10 mM HEPES, 3 mM Mg-ATP, 0.3 mM Na_3GTP, and 5 mM QX-314 (pH 7.25) (280 to 300 milliosmoles [mOsm]) for recording miniature excitatory postsynaptic currents (mEPSCs) with 50 μM picrotoxin and 1 μM tetrodotoxin (TTX) in ACSF and contained 130 mM K-gluconate, 5 mM NaCl, 1 mM $MgCl_2$, 0.05 mM EGTA, 10 mM HEPES, 3 mM Mg-ATP, and 0.3 mM Na_3GTP (pH 7.25) (280 to 300 mOsm) for recording passive membrane properties. Long-term potentiation (LTP) was induced by four trains of 100 Hz lasting 1 s each, with a 20-s intertrain interval, and long-term depression (LTD) was induced either by application of 100 μM (*RS*)-3,5-dihydroxyphenylglycine [(*RS*)-3.5-DHPG] for 10 min (for mGluR-LTD) or by low-frequency stimulation consisting of 900 stimuli delivered at 1 Hz (for NMDAR [*N*-methyl-D-aspartic acid receptor]-LTD). All data acquisition and analysis were done using pClamp 9 software (Molecular Devices, Union City, CA). The ages of the mice ranged from 13 to 17 days for NMDAR-LTD, 3 to 5 weeks for mGluR-LTD, mEPSCs, and membrane properties, and 8 to 10 weeks for all other field recordings.

Primary hippocampal culture and immunostaining. Previously described procedures for the preparation of cultured hippocampal neurons, immunostaining, and image collection and analysis (38) were followed with minor modifications. Briefly, neuronal cultures were prepared from postnatal day 1 (P1) and maintained in neurobasal A/B27 medium. Whenever possible, the DK cultures were prepared together along with the WT littermates on the same 24-well plates for better comparison. A standard procedure for preparation and infection of cultured neurons by helper phage-dependent adenoviruses expressing enhanced green fluorescent protein (EGFP) and PAK3 was followed (51). Cell-permeable cofilin peptides [reverse control, NFVKIVGDSVAVGSAMRQIKIWFQNRRM KWKK; pS3, MAS(p)GVAVSDGVIKVFNRQIKIWFQNRRMKWKK, >99% purity] were made by Biomatik (Canada) and used as described previously (1). For analysis of dendrite and axon growth, neurons were fixed at day *in vitro* (DIV) 3, 7, 14, or 21 with 4% paraformaldehyde-PBS, permeabilized with 0.1% Triton X-100–PBS, blocked with 5% fetal bovine serum, and then incubated in various primary antibodies followed by appropriate secondary antibodies. For F-actin labeling, following the secondary antibodies, the cells were further stained with 1 μg/ml tetramethylrhodamine isothiocyanate (TRITC)-conjugated phalloidin (Sigma, St. Louis, MO). Images were collected using a Zeiss LSM 510 confocal microscope (63× objective for dendritic and synaptic staining) or Nikon TE2000 histology microscope (20× objective for axonal staining), under identical gain and contrast settings for the WT and DK samples. The spines were defined as mushroom (head/neck ratio of >2.5), thin (head/neck ratio of >1 but <2.5), filopodia (no distinguishable head; length, >5 μm), or stubby (no distinguishable neck). Unless otherwise specified, all summary data involving cultured neurons were collected from a total of 15 to 30 neurons from at least three independent hippocampal cultures. All measurements were quantified using either Zeiss LSM Image Browser or ImageJ. Primary antibodies used in immunostaining included anti-phospho-neurofilament (Sternberg Inc.), anti-MAP2 (Millipore), antisynaptophysin (Sigma), anti-GluR2/3 (Chemico), and anti-GFAP (Dako).

Behavior tests. The general training, testing paradigms, and data analyses for open-field, fear conditioning, and water maze tests were described previously (38, 39), with some modifications. Briefly, TruScan 2.0 (Coulbourn Instrument, Whitehall, PA) was used to acquire and analyze the locomotion activities. For fear-learning and memory tests, the prehandled animals were placed in a chamber (22.5-cm-wide by 32.5-cm-long by 33.3-cm-high Plexiglas cage with a grid floor, encased in an isolation cubicle) and allowed to explore the cage for the first 120 s, after which a 30-s white noise tone was delivered followed by a 2-s, 0.7-mA foot shock. Three such training sessions were delivered in succession, with 30-s intertrain intervals. Following 2 and 24 h after the training, mice were tested for short-term and long-term fear memory, respectively. In the contextual test, mice were returned to the same chambers in which they were trained and their freezing response was analyzed over the course of 4 min. In cued tests, the mice were placed in a separate chamber with an entirely different context and allowed to explore for 120 s, after which the tone was delivered for the next 120 s. All data were analyzed using FreezeView2 (Coulbourn Instrument, Whitehall, PA). Freezing was defined as a motion index of 25 or less. For the water maze test, the acquisition phase consisted of 5 training days with four trials every day, and the probe trial was given 1 h and 24 h after the last training session to assess short-term and long-term memory, respectively. The spatial memory for the platform location was evaluated by the analysis of the dwelling time in the platform zone (a 20-cm-diameter circular area in which the platform was centered). The swim path was recorded by a camera connected to a video tracking system (Noldus Information Technology) and analyzed with EthoVision software. The elevated plus maze (57) consisted of four arms (two open arms without walls and the other two enclosed by 15.25-cm-high walls) 30 cm long and 5 cm wide. Each arm was attached to sturdy legs such that they were elevated 50 cm off the ground surface. To initiate the test, a mouse was placed on the edge of an open arm, and once the mouse reached the maze center, the data recording started and the mouse was given 5 min to explore the maze. The arm entry and the time spent in each arm in the maze center were recorded manually. For all behavioral tests, only male mice between the ages of 2 to 4 months were used, and the experiments were performed during the light phase of the cycle (between 9:00 a.m. and 2:00 p.m.). All animals were handled 3 times daily for 2 days before any behavioral tests.

Data analysis. All the data were analyzed with Student's *t* test, and *P* values of less than 0.05 were regarded as statistically significant (indicated with an asterisk in summary graphs). Values were presented as means ± standard errors of the means (SEM).

RESULTS

Selective deficit in postnatal brain growth in PAK1/PAK3 DK mice. Since PAK1 and PAK3 are coexpressed in the developing brain (7, 24, 39) and share some biochemical properties (5, 11, 60), we reasoned that they might have redundant functions during brain development. Therefore, we generated and analyzed PAK1/PAK3 double-knockout mice (DK) mice. The DK mice were born healthy, with normal brain mass (WT = 93.0 ± 1.6 mg, DK = 91.1 ± 1.7 mg, $P = 0.45$) at birth (Fig. 1B and C). However, the DK brain failed to grow normally (Fig. 1A and C), resulting in a marked reduction in brain volume and mass at maturity (2 to 4 months) (WT = 413 ± 6 mg, DK = 255 ± 8 mg [38.3% reduction compared to WT], $P < 0.0001$). The body weights of the DK mice were not affected at birth or maturity. Histological Fluoro Nissl staining of brain sections also indicated that the DK brain was smaller at maturity than the WT brain (Fig. 1D) but normal at birth (Fig. 1E). To determine which brain regions were affected, we carried out magnetic resonance imaging (MRI) analysis of the whole brain and found that all identifiable regions were significantly reduced in the DK brain (Fig. 1F to I). Specifically, the whole-brain volume of the DK brain was reduced by 36.0% (WT = 432.3 ± 23.2 mm^3, DK = 276.6 ± 8.7 mm^3, $P < 0.0001$), the frontal cortex by 35.4% (WT = 36.02 ± 3.05 mm^3, DK = 23.23 ± 1.00 mm^3, $P < 0.0001$), and the hippocampus by 34.5% (WT = 19.43 ± 1.05 mm^3, DK = 12.72 ± 0.51 mm^3, $P < 0.0001$) (Fig. 1I). Coronal MRI sections of frontal cortices depicted not only reduced cortical thickness but also notably thinner corpus callosa (Fig. 1G, arrows) (WT = 19.23 ± 1.35 mm^3, DK = 11.73 ± 0.81 mm^3 [39.0% reduction]) and smaller medullas and spinal cords (Fig. 1H, arrows) in the DK mice. Therefore, PAK1/PAK3 DK mice exhibit a robust secondary microcephaly phenotype, providing a clinically relevant model for studying the mechanisms underlying this brain disorder.

Hyperactivity, increased anxiety, and learning deficits in PAK1/PAK3 DK mice. Clinical studies show that *PAK3*-linked mental retardation patients display hyperactivity, excessive anxiety, restlessness, and impaired spatial memory (3, 46). Therefore, to assess whether PAK1/PAK3 DK mice possess these clinical features, we carried out the following behavioral tests. First, we used an open-field test to evaluate spontaneous exploration of a new environment and locomotor activity of the mice (Fig. 2A). The DK mice traveled longer distances (WT = 3.4 ± 0.4 m, DK = 6.8 ± 0.4 m, $P < 0.0001$), exhibited greater movement velocity (WT = 68 ± 8 cm/min, DK = 136 ± 7 cm/min, $P < 0.0001$), and had reduced rest time (WT = 16.5 ± 2.0 s, DK = 6.5 ± 1.9 s, $P < 0.005$). Thus, the DK mice are more active in locomotor behaviors. Second, we evaluated anxiety levels of the mice by using an elevated plus maze. In WT mice, open-arm entries constituted 55.8% ± 3.7% of total arm entries, which were greatly reduced and constituted only 16.5% ± 3.6% of total arm entries (Fig. 2B) ($P < 0.001$) in the DK mice. While both WT and DK mice spent comparative amounts of time in the maze center (WT = 29.2% ± 1.2%, DK = 26.7% ± 2.3%, $P > 0.05$) (Fig. 2C), DK mice spent significantly less time exploring the open arms and more time exploring the closed arms (time spent in open arms, WT = 39.2% ± 1.2%, DK = 15.4% ± 4.3%, $P < 0.001$) (Fig. 2C). These results indicated that the DK mice are more anxious than the WT control. Finally, to evaluate the cognitive performance, we employed two independent learning paradigms: fear conditioning and water maze. In the fear conditioning tests, both WT and DK mice showed low levels of freezing prior to the foot shock (WT = 13.8% ± 3.4%, DK = 11.8% ± 3.2%, $P > 0.5$) and equally increased the freezing after the foot shock (WT = 40.2% ± 9.4%, DK = 34.2% ± 7.0%, $P > 0.5$) (Fig. 2D), indicating that the DK mice were not altered in ability to freeze in response to a foot shock. However, the memory test carried out 1 h after the training showed profound deficits in the DK mice. The DK mice displayed greatly reduced freezing compared to the WT control in both cued (WT = 46.8% ± 8.3%, DK = 10.2% ± 2.2%, $P < 0.001$) (Fig. 2E) and contextual (WT = 49.9% ± 8.4%, DK = 11.8% ± 2.2%, $P < 0.001$) (Fig. 2F) tests. In fact, the levels of freezing in DK mice before and after the tone (or during the contextual test) were the same (cued test, 10.2% ± 2.2%, *P* value of >0.05 compared to pretone; contextual test, 11.8% ± 2.2%, *P* value of >0.05 compared to basal freezing before training). These results indicate a complete abolishment of fear memory in the DK mice. To confirm the memory deficit, we also performed the Morris water maze test to specifically assess spatial learning and memory. The distance and latency to reach the platform were quantified over 5 days of training and showed that by the third day of training, both the average swim distance (e.g., on day 5, WT = 290 ± 30 cm, DK = 720 ± 86 cm, $P < 0.005$) (Fig. 2G) and the average latency (WT = 11.3 ± 1.33 s,

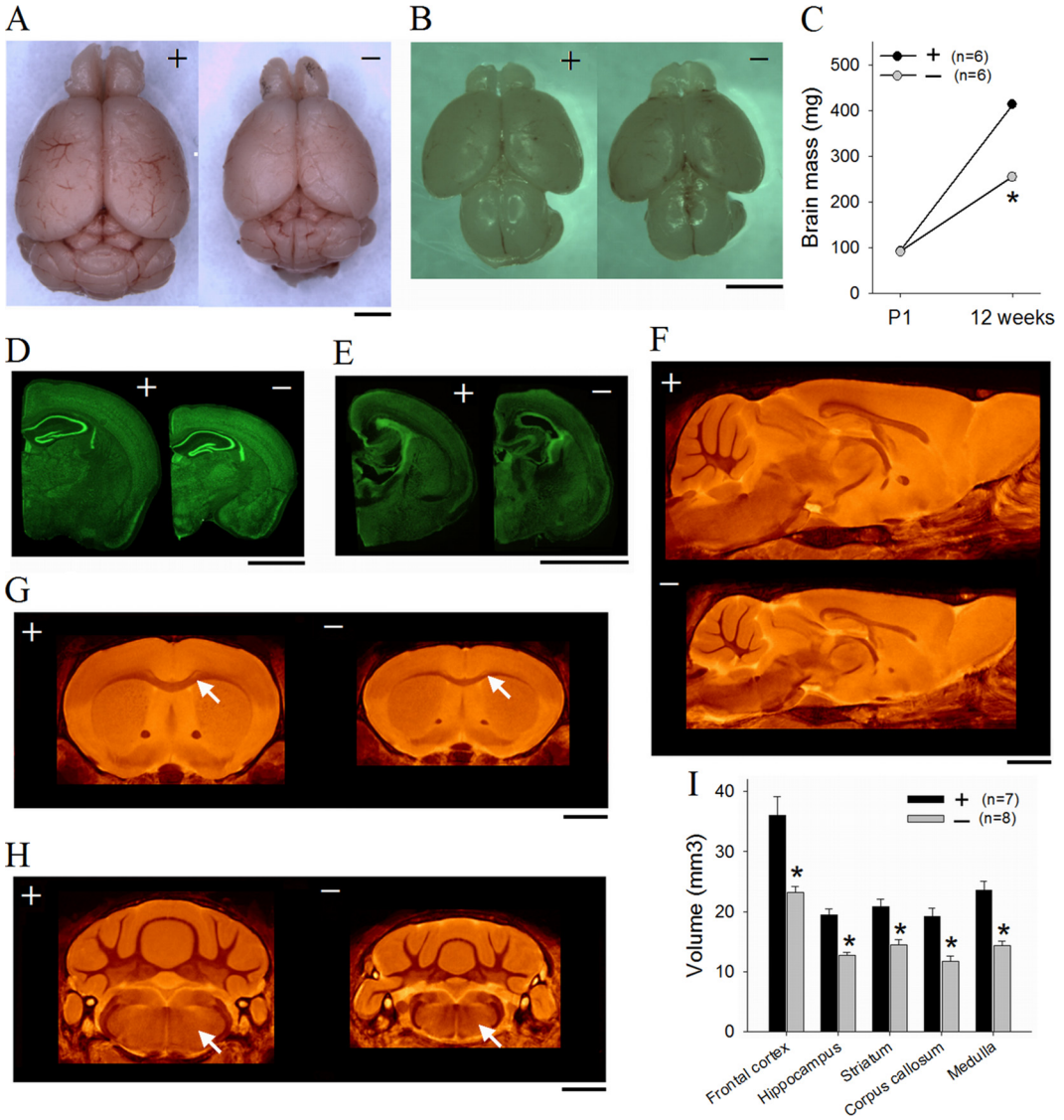

FIG. 1. Defect in postnatal brain growth in PAK1/PAK3 DK mice. (A, B) Pictures showing reduced brain size in the DK (labeled with a minus sign in all figures) mice compared to that of the WT (labeled with a plus sign in all figures) littermates at maturity (A) but not at birth (B). (C) Summary graph showing reduction in brain mass at 12 weeks but not at birth in the DK mice (n = number of animals). (D, E) Fluoro Nissl staining of brain sections showing reduced brain size in DK mice at maturity (D) but normal size at birth (E). (F) Sagittal planes of averaged MRI atlas of adult brains illustrating reduced size in DK mice. (G, H) Coronal MRI sections depicting reduced cortical thickness and thinner corpus callosum (G, arrows) and smaller medulla and spinal cord (H, arrows) in the DK brain. (I) Averaged volumes for selected brain regions (n = number of animals). Bars, 2 mm.

DK = 29.8 ± 3.1 s, $P < 0.0001$) of the DK mice became significantly greater than those of the WT control. Probe tests carried out 1 h (WT = 6.89 ± 1.27 s, DK = 2.61 ± 0.65 s, $P < 0.01$) (Fig. 2H) or 24 h (WT = 5.48 ± 0.83 s, DK = 1.94 ± 0.27 s, $P < 0.001$) after day 5 of training showed that the DK mice spent significantly less time exploring the target zone than the WT mice. The swim speed showed no differences between the WT and DK mice (WT = 24.26 ± 0.63 cm/s, DK = 22.89 ± 0.64 cm/s, $P > 0.05$) (Fig. 2I), indicating that motor function was not impaired in the DK mice. To determine whether the deficit in the water maze performance was related to vision or motivation to find the platform, we also performed the visible-platform test but found no significant differences between the WT and DK mice (data not shown). These results indicate that PAK1/PAK3 DK mice are profoundly impaired in learning and memory performances. It is important to emphasize that single-KO mice lacking either PAK1 or PAK3 exhibited no significant deficits in either open-field or fear memory tests and only mild deficits in an aversive-taste test (39), indicating that, similar to brain size regulation, PAK1 and PAK3 are also functionally redundant in the regulation of behavioral plasticity.

Taken together, these behavioral tests further validated the PAK1/PAK3 DK mice as a clinically important model for secondary microcephaly and mental retardation.

Normal anatomical and cellular organization but increased cell density in the DK mice. To investigate the underlying causes for the reduced brain size in the DK mice, we first

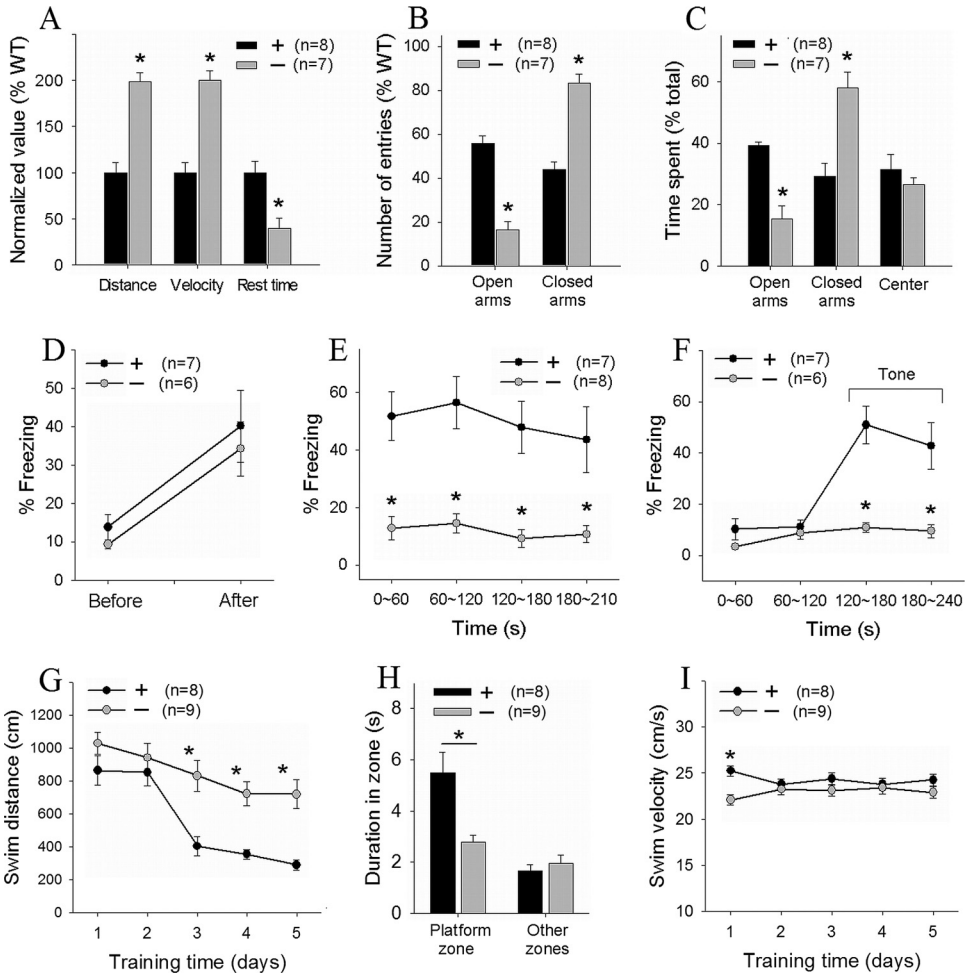

FIG. 2. Altered behaviors and impaired learning and memory in PAK1/PAK3 DK mice. (A) Open-field test showing increased travel distance and speed and reduced rest time in the DK mice. (B, C) Elevated plus maze test showing decreased open-arm entries (B) and total time spent in the open arms (C) in the DK mice. (D) Fear memory training phase showing similar responses between genotypes before and after the tone/shock presentation. (E and F) Fear memory test carried out 1 h after the training, showing lack of freezing in both contextual (E) and cued (F) tests in the DK mice. (G) Learning acquisition phase in the hidden-platform water maze test, showing prolonged swim distances to locate the platform in the DK mice. (H) Probe test carried out 1 h after the fifth day of water maze training, showing reduced time to explore the target zone in the DK mice. (I) Swim speed showing no significant differences between genotypes. n = number of animals.

examined whether the number and/or organization of the brain cells were altered. Previous studies using cultured neurons or other cell lines suggest that PAKs may be involved in cell proliferation (53, 55), survival (37), and/or migration (13, 50), and therefore, it is possible that the absence of PAK1/PAK3 may lead to defects in any of these processes, resulting in reduced neuronal number and/or abnormal cellular organization. However, as shown in Fig. 3A, although the cortical thickness was clearly reduced, all the cortical layers appeared to be present in the DK mice. This was confirmed by immunostaining experiments using the layer-specific marker Cux1 (upper layers) (Fig. 3B) and Tbr1 (deep layers) (Fig. 3C). Golgi impregnation also showed a similar pattern of layer organization and neuronal polarity (Fig. 3D). However, a magnified view of cresyl violet staining of layer IV of the frontal cortex (Fig. 3E) revealed that neurons in the DK mice were more densely packed and had smaller cell bodies than those of WT mice (neuronal cell body cross-sectional area, WT = 219.6 ± 3.8 μm^2, DK = 131.1 ± 2.1 μm^2, $P < 0.0001$). Increased neuronal density with reduced soma was also observed throughout hippocampal CA1, CA3, and dentate gyrus regions. These results suggested that the total cell number might not be greatly affected in the DK mice. To examine this more thoroughly, we performed stereological counting using the optical fractionator approach and estimated the density and the total neuron count in the cortex (Fig. 3F and G). As expected, the neuronal density was significantly higher (by 32%) in the DK mice (WT = $1.71 \times 10^5 \pm 1.03 \times 10^3$ neurons per mm^3, DK = $2.25 \times 10^5 \pm 1.19 \times 10^3$ neurons per mm^3, $P < 0.0001$). Notably, total cortical neuron count was only slightly affected in the DK cortex (WT = 1.83 ± 0.06×10^7 neurons, DK = 1.64 ± 0.05 $\times 10^7$ neurons). Similarly, the density of hippocampal glias was also significantly increased in the DK mice (WT = 124.4 ± 4.2 glias per mm^3, DK = 188.0 ± 5.5 glias per mm^3, $P < 0.0001$) (Fig.

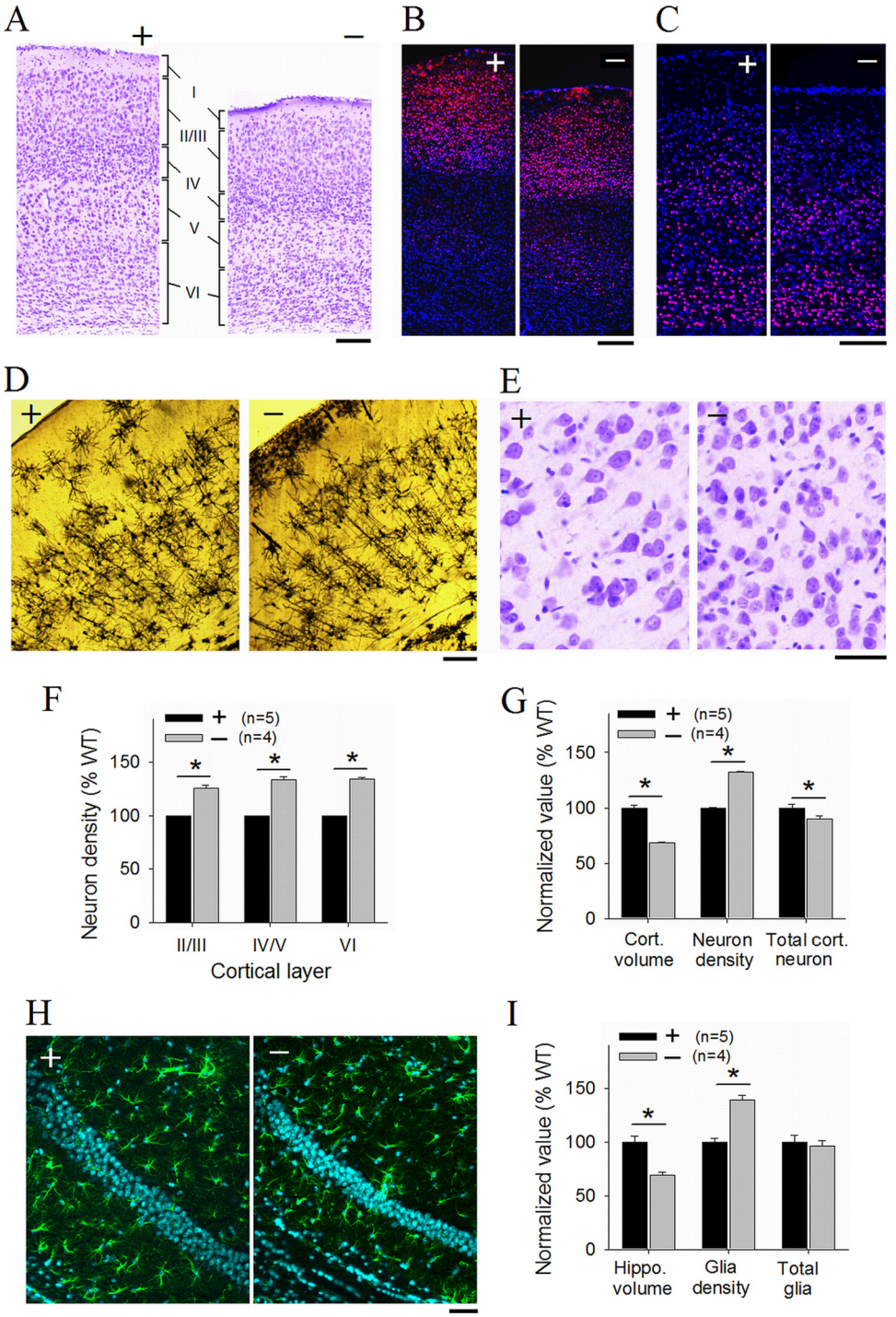

FIG. 3. Increased neural and glial cell density in PAK1/PAK3 DK mice. (A) Cresyl violet staining of the frontal cortices showing normal cortical layers. (B, C) Cortical sections stained with the upper-layer-specific marker Cux1 (B) and the deep-layer-specific marker Tbr1 (C). (D) Golgi impregnation showing normal neuronal polarity in the frontal cortex. (E) Magnified view of cresyl violet-stained regions (layer IV, frontal cortex) revealing smaller and more densely packed neurons in the DK cortex. (F and G) Summary graphs of optical fractionator measurements, showing increased cell density in individual cortical layers (F) and in the entire cortex (G) (n = number of animals). (H) GFAP-DAPI-costained hippocampal CA1 areas showing increased cell density for both CA1 neurons and glia. (I) Summary graph of optical fractionator measurements on GFAP-DAPI-costained hippocampal sections showing reduced hippocampal volume and increased glia density without changes in total glia counts in the DK mice (n = number of animals). Scale bars, 200 μm (A to D) and 50 μm (E and H).

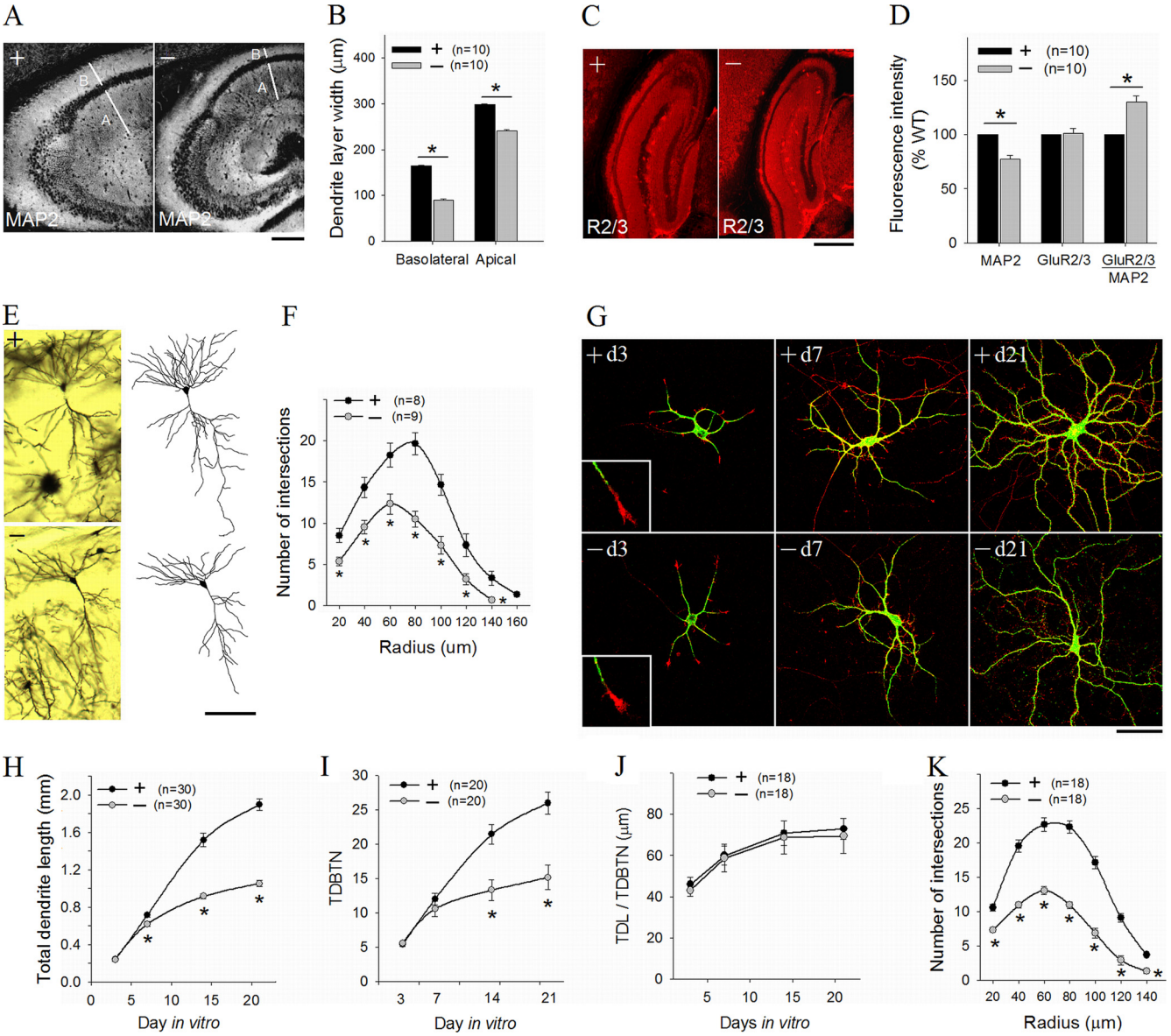

FIG. 4. Reduced dendritic arborization in PAK1/PAK3 DK mice. (A, B) Hippocampal sections stained for the dendritic marker MAP2 (A) and summary data (B), showing reduced width for both basolateral and apical dendritic fields in the CA areas of the DK mice. Scale bar, 200 μm. (C) Hippocampal sections stained for AMPA receptor GluR2/3. Scale bar, 500 μm. (D) Summary data showing reduced fluorescence intensity for MAP2 but not for GluR2/3 in the DK mice (n = number of brain sections). (E) CA1 pyramidal neurons with Golgi impregnation (left) and camera lucida drawings (right) showing reduced dendritic complexity in the DK mice. Scale bar, 100 μm. (F) Sholl analysis of CA1 neurons, showing a reduced number of intersections across all radii (n = number of reconstructed neurons). (G) Cultured hippocampal neurons stained for MAP2 (green) and F-actin (phalloidin [red]), showing reduced dendritic complexity at DIVs 15 and 21 but not at DIV 3 and 7 in the DK mice. Scale bar, 50 μm. (H to J) Summary data of cultured hippocampal neurons at DIV 21, showing reduction in the total dendritic length (H) and total dendritic branch tip number (TDBTN) (I) but not in the average length of individual dendrites (J) in the DK mice. (K) Sholl analysis of hippocampal neurons at DIV 21 showing deficits in dendritic arborization. n = number of neurons.

3H), and the total glial counts were comparable between the genotypes (WT = 2,417 ± 154, DK = 2,391 ± 119, $P = 0.90$) (Fig. 3I).

Reduced dendritic arbors and axons in PAK1/PAK3 DK mice. A small reduction in cell number along with increased cell density suggest that neurogenesis is not the main cause for the reduced brain growth in the DK mice. Interestingly, both PAK1 and PAK3 are expressed mainly in postmitotic neurons, implying specific roles in neuronal morphogenesis and maturation (24, 39, 44, 61). Indeed, a number of studies using cultured neurons have shown that PAK1 is involved in neurite formation and outgrowth (23, 25), but whether they are important in *in vivo* dendritic development is unknown. Staining for the dendritic marker MAP2 showed a clear reduction in the size of the dendritic field in the hippocampus (basolateral CA1 width, WT = 164.1 ± 1.3 μm, DK = 90.3 ± 1.5 μm, $P < 0.0001$; apical CA1 width, WT = 298.4 ± 1.7 μm, DK = 241.3 ± 2.5 μm, $P < 0.0001$) (Fig. 4A and B). In addition, the

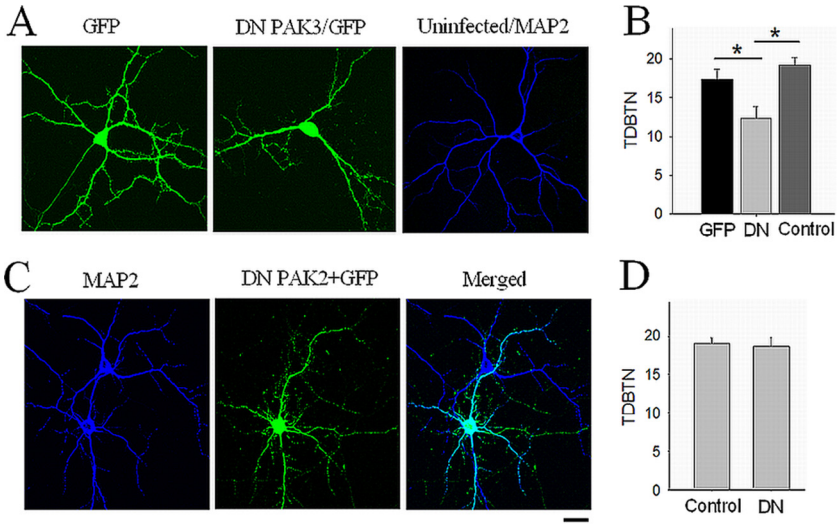

FIG. 5. Effect of dominant negative (DN) PAK3 and PAK2 on neuronal complexity. (A) Cultured hippocampal neurons prepared from PAK1 KO pups infected with viruses expressing GFP or DN GFP-PAK3 showing reduced dendritic arbors in DN PAK3 virus-infected but not GFP PAK3 virus-infected neurons. (B) Summary graph showing reduction in neuronal TDBTN in DN PAK3 virus-infected neurons compared to the noninfected control or GFP virus-infected neurons ($n = 20$ neurons for each treatment). (C) Cultured hippocampal neuron prepared from PAK1 KO pups cotransfected with DN PAK2 (K278R) and GFP (green) plasmid DNA, showing dendritic arbors similar to that of untransfected neuron (blue; MAP2). (D) Summary graph showing no differences in neuronal TDBTN between DN PAK2-transfected and untransfected neurons. Bar, 20 μm.

MAP2 fluorescence intensity per dendritic area was significantly reduced in the DK mice (DK = 77.6% ± 3.2% of WT, $P < 0.0001$) (Fig. 4D). Interestingly, despite the reduction in MAP2 staining, the relative fluorescence intensity for glutamate receptor GluR2/3 was significantly increased (ratio of GluR2/3 to MAP2, DK = 130.2% ± 5.51% of WT, $P < 0.0001$) (Fig. 4C and D; also see below). Golgi impregnation of fixed brain sections showed that the dendritic complexity of both cortical and hippocampal pyramidal neurons were greatly reduced in the DK mice (Fig. 4E). Sholl analysis of camera lucida-reconstructed CA1 neurons confirmed the reduction in the dendritic arbors in the DK mice (Fig. 4F). To test whether the dendritic defect was an intrinsic property of the neurons rather than being due to an altered brain environment, we analyzed cultured hippocampal neurons. In the early days of the culturing, both the growth cone morphology and dendritic growth appeared to be normal in DK neurons (Fig. 4G to I). For example, at day 3 *in vitro*, both the numbers and total lengths of the dendrites were identical between WT and DK neurons (WT = 248 ± 10 μm, DK = 241 ± 17 μm, $P = 0.78$) and only slightly different at day 7 (WT = 719 ± 23 μm, DK = 620 ± 26 μm [87% of WT], $P = 0.03$). However, dendritic arbors became increasingly simpler at later stages of development (on day 14, WT = 1,518 ± 72 μm, DK = 917 ± 25 μm [61% of WT], $P < 0.0001$; on day 21, WT = 1,894 ± 62 μm, DK = 1,054 ± 30 μm [56% of WT], $P < 0.0001$). Sholl analysis confirmed profound deficits in dendritic arborization in mature DK neurons (Fig. 4K). It is interesting to note that although the number of intersections and total dendritic length were reduced in the DK neurons, the average lengths of individual dendrites were the same between the WT and DK neurons (Fig. 4J), indicating that PAK1 and PAK3 are specifically important for dendritic branching. The cell body of the DK neurons at day 21 was also significantly smaller than that of the WT neurons (cell body cross-sectional area, WT = 286.0 ± 15.3 μm^2, DK = 150.4 ± 6.9 μm^2, $P < 0.001$). To independently verify this dendritic defect, we expressed the dominant negative (DN) PAK3 or PAK2 in PAK1 KO neurons. The dendritic growth and complexity of the PAK1 KO neurons are normal (7). As shown in Fig. 5A and B, DN PAK3/GFP virus-infected but not GFP virus-infected neurons showed significantly reduced dendritic arbors, as seen in the DK neurons. Interestingly, the expression of DN PAK2 had no effect on the dendritic growth of PAK1 KO neurons (Fig. 5C and D). Therefore, the reduced dendritic arborization in DK mice is likely a direct consequence of PAK1/PAK3 deletion and not a secondary chronic effect of the genetic manipulations.

Like dendrites, axons are major structural components of the neurons; however, the contribution of axon abundance to brain volume is unclear. Previous studies in invertebrates have implicated PAKs in the regulation of axon guidance and growth (4, 20, 26, 28, 33), but little *in vivo* data are available in vertebrates. Interestingly, our MRI data (Fig. 1) showed that the DK mice had particularly reduced white matter tracts compared to those of WT mice, suggesting that axonal properties are also altered in these mice. To address this possibility, we first performed immunostaining for myelin (a marker for myelinated axons) and found that stained areas were significantly reduced throughout the DK brain (Fig. 6A). Analysis of myelin fluorescence showed that white matter volume was profoundly reduced in the DK brain compared to that of the WT brain (total fluoromyelin intensity across cortex, DK = 57.3% ± 5.1% of WT, $P < 0.0001$). The staining patterns appeared to be similar for the WT and DK brains, suggesting that axonal guidance/connectivity was likely unaffected in the DK mice. To specifically examine the hippocampal areas, we performed immunostaining using the axon-specific marker phospho-neurofilament (pNF) and found a striking reduction in the amount of

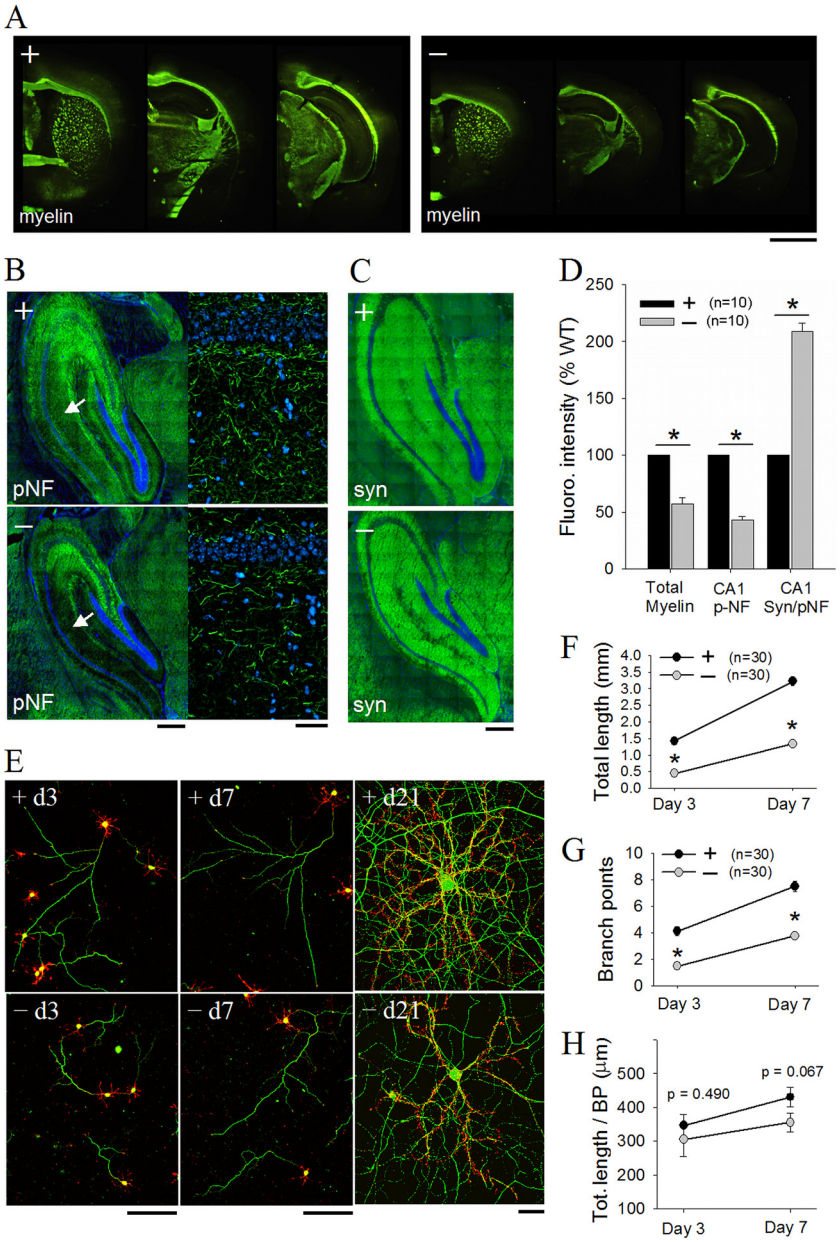

FIG. 6. Reduced axonal growth in PAK1/PAK3 DK mice. (A) Brain sections stained for myelin showing thinner white matter tracts in the DK mice. Scale bar, 2 mm. (B) Hippocampal sections stained for the axon-specific protein phospho-neurofilament (pNF) revealing reduced pNF fluorescence intensity in the CA1 area (arrow) in the DK mice. Scale bar, 300 μm. On the right are enlarged CA1 dendritic areas revealing reduced axonal fragments in the DK section. Scale bar, 50 μm. (C) Hippocampal sections stained for the presynaptic marker synapsin (syn). Scale bar, 300 μm. (D) Summary data showing reduced fluorescence intensity of myelin and pNF but not of synapsin in the DK mice (n = number of brain sections). (E) Cultured hippocampal neurons stained at DIVs 3, 7, and 21 for pNF (green) and F-actin (red) showing reduced axonal growth in DK neurons. Scale bars, 50 μm. (F to H) Summary data showing reduction in both total axon length (F) and branching points (G) but not in average branch length (H) in the DK neurons (n = number of neurons).

fluorescence in the Schaffer collateral area in the DK mice (normalized pNF immunofluorescence intensity, DK = 42.9% ± 3.2% of WT, $P < 0.0001$) (Fig. 6B and D). In contrast, despite the drastic reduction in pNF staining fluorescence, the relative fluorescence intensity of the presynaptic marker synaptophysin was significantly increased in the DK brain (ratio of synaptophysin to pNF fluorescence intensity, DK = 214% ± 7.5% of WT, $P < 0.0001$) (Fig. 6C and D). The relative increase in synaptophysin expression in the DK mice was similar to that of postsynaptic glutamate receptors (Fig. 4A to D), suggesting altered synaptic properties (see below). To further determine the nature of the axonal deficit, we again used cultured hippocampal neurons costained for pNF and F-actin to track the development of the axons (Fig. 6E to H). Both WT and DK neurons had only one primary axon, indicating that axon specification is not disturbed. However,

at days 3 and 7, the DK neurons showed a clear reduction in both total axon length (on day 3, WT = 1,426 ± 75 μm, DK = 451 ± 40 μm, $P < 0.0001$; on day 7, WT = 3,230 ± 131 μm, 1,340 ± 52 μm, $P < 0.0001$) (Fig. 6F) and the number of branching points (on day 3, WT = 4.12 ± 0.33, DK = 1.48 ± 0.20, $P < 0.0001$; on day 7, WT = 7.50 ± 0.40, DK = 3.77 ± 0.26, $P < 0.0001$) (Fig. 6G). The effect on the mean length of individual branches was mild and not significant (Fig. 6H), suggesting that the primary role of PAK1 and PAK3 in axonal development is to promote axonal branching.

In clear contrast to the neuronal defects, analysis of glial cells in hippocampal sections stained for the glia-specific marker GFAP indicated that the morphologies of these cells were indistinguishable between WT and DK mice (cell body area, WT = 55.6 ± 2.5 μm^2, DK = 56.7 ± 3.6 μm^2, $P > 0.05$; number of primary processes, WT = 5.7 ± 0.2, DK = 5.4 ± 0.4, $P > 0.05$; total process length, WT = 121 ± 1.9 μm, DK = 124 ± 2.2 μm, $P > 0.05$). Thus, the morphological defects in the DK mice are specific to the neurons.

Taken together, these results indicate that PAK1 and PAK3 are critically required for dendritic/axonal branching, which likely represents a key mechanism by which PAK1 and PAK3 promote postnatal brain enlargement.

Enhanced basal synaptic transmission and reduced synaptic plasticity in PAK1/PAK3 DK mice. To investigate the functional consequences of reduced neuronal complexity and smaller brain on neuronal and synaptic properties, we performed electrophysiological recordings in the CA1 region of the hippocampus. First, we analyzed the membrane properties of CA1 neurons using whole-cell recordings and found that, compared to WT neurons, the DK neurons exhibited increased input resistance and reduced current injections needed to elicit an action potential (Fig. 7A and B). These changes are consistent with the morphological data showing that the DK neurons are smaller and simpler than WT neurons. The resting membrane potential, access resistance, threshold to fire an action potential, or the amplitude of the action potential were not affected (Fig. 7C to E). Second, we evaluated basal synaptic strength at CA1 synapses by stimulating the Schaffer collateral fiber. Input-output curves of field excitatory postsynaptic potentials (fEPSPs) showed drastically enhanced responses over a wide range of stimulus intensities in DK slices (Fig. 7F to H). The enhanced synaptic transmission was surprising because of the markedly reduced dendritic arbors and axons, which could predict fewer synapses and thus reduced synaptic responses. In contrast to the elevated basal synaptic function, the DK mice were impaired in synaptic plasticity. Both long-term potentiation (LTP) and depression (LTD) were significantly attenuated in DK mice (Fig. 7I to K). In particular, both NMDA receptor-dependent (Fig. 7J) and metabotropic glutamate receptor-dependent (Fig. 6K) LTD were nearly completely abolished in the DK mice (WT = 72.8% ± 4.6%, DK = 88.8% ± 3.9%, $P < 0.024$, and WT = 79.3% ± 1.7%, DK = 94.5% ± 2.9%, $P < 0.001$, respectively). These results indicate that the reduced neuronal complexity has profound effects on overall basal synaptic efficacy and ability to undergo bidirectional synaptic plasticity. Since both LTP and LTD are thought to be important cellular mechanisms underlying learning and memory (35), their deficits may contribute to the cognitive deficits of the DK mice.

Reduced synapse density but enlarged individual synapses in PAK1/PAK3 DK mice. To determine how the reduced dendritic arbors and axons lead to enhanced basal synaptic transmission, we first analyzed the properties of the dendritic spine, the major site of excitatory synaptic input. Analyses of cortical and hippocampal pyramidal neurons with Golgi impregnation revealed that the DK mice were profoundly altered in spine morphology (Fig. 8A and B). For example, the DK mice had significantly fewer mushroom-shaped spines than the WT mice (WT = 48.7% ± 3.2%, DK = 20.0% ± 1.5%, $P < 0.0001$) (Fig. 8C), more filopodia (WT = 8.4% ± 1.0%, DK = 27.3% ± 2.1%, $P < 0.0001$) (Fig. 8C), reduced head/neck ratios (Fig. 8D), smaller spine head areas (Fig. 8E), and increased spine length (Fig. 8F). In particular, the DK neurons displayed over a 10-fold increase in the number of uncommon spines characterized by the existence of spine protrusions or branches on the spine head (WT = 1.31% ± 0.05%, DK = 15.33% ± 1.12%, $P < 0.0001$) (Fig. 8B and C). The density of the total dendritic protrusions (including all types of spines), however, was not significantly altered in DK mice (number of spines per 10-μm dendritic segment, WT = 7.02 ± 0.25, DK = 6.60 ± 0.22, $P = 0.24$). Analysis of cultured hippocampal neurons prepared from the DK mice also showed similar spine deficits. These results indicate that PAK1 and PAK3 are essential for normal spine morphology.

To further investigate the effect of PAK1/PAK3 deletion on synaptic properties, we analyzed both synapse density and the structure of individual synapses. Immunostaining experiments showed that the relative levels of both postsynaptic glutamate receptors (Fig. 4) and presynaptic marker synaptophysin (Fig. 6) were elevated in the DK hippocampal area, suggesting that either the synapse density and/or synaptic properties of individual synapses are enhanced. The former possibility is unlikely given the reduced dendritic arbors/axons and normal spine density per unit of dendrite in the DK mice. To confirm this, EM thin sections of the hippocampal CA1 area were obtained and analyzed. As shown in Fig. 9, the density of asymmetric synapses (Fig. 9A, arrowheads) (identified by the presence of postsynaptic density [PSD] apposed to presynaptic vesicles) was indeed significantly reduced in the DK sections compared to that of the WT sections (WT = 34.63 ± 0.94/100 μm^2, DK = 26.28 ± 0.71/100 μm^2, $P < 0.001$) (Fig. 9A and C). However, analysis of the PSD length indicated that the size of PSD was significantly increased in the DK mice (Fig. 9A and B). To further examine the property of individual synapses, we analyzed cultured neurons costained for the combination of the presynaptic marker synaptophysin, postsynaptic glutamate receptor GluR2/3, the spine marker F-actin, and the axonal marker pNF. WT neurons were characterized by complex axonal networks interposed with elaborate dendritic trees, with more but relatively weaker synaptophysin puncta (Fig. 9D, left), whereas the DK neurons had simpler axonal networks interposed with less-complex dendritic trees with apparently larger and stronger synaptophysin-stained puncta (Fig. 9D, right). Analysis of randomly selected dendritic segments showed that although the numbers of synaptophysin puncta per unit of dendritic length were the same between WT and DK neurons (WT = 6.9 ± 0.3/10 μm, DK = 6.9 ± 0.2/10 μm,

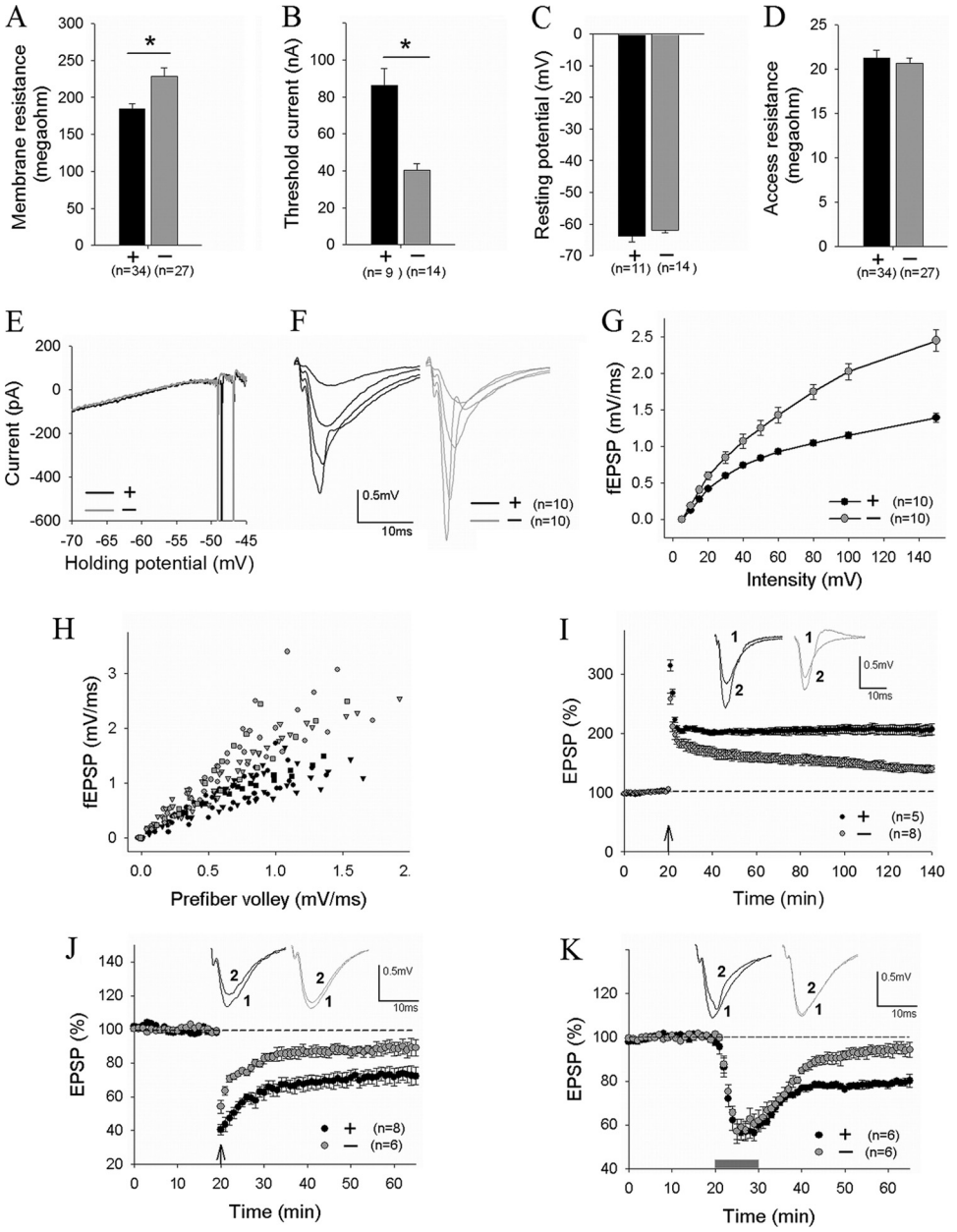

FIG. 7. Enhanced basal synaptic strength and impaired synaptic plasticity in PAK1/PAK3 DK mice. (A to D) Whole-cell recordings of CA1 pyramidal neurons showing increased input resistance (A) and decreased current injections to elicit an action potential (B) but normal resting membrane potential (C), access resistance (D), and threshold potential to fire an action potential (E) in the DK neurons. (F to H) fEPSPs at CA1 synapse (F) and summary graphs (G and H) evoked by various stimulation intensities showing enhanced synaptic responses in the DK mice. (I, J, and K) fEPSP recordings showing significantly reduced NMDA receptor-dependent LTP induced by high-frequency stimulation (4 times at 100 Hz, lasting 1 s each, arrow) (I), diminished NMDA receptor-dependent LTD induced by 1-Hz stimulation (15 min) (J, arrow), and the abolishment of metabotropic glutamate receptor (mGluR)-dependent LTD induced by brief (10-min) application of 100 μM group I mGluR agonist DHPG (K, bar). n = number of slices or neurons.

$P = 0.94$) (Fig. 9E and F), the sizes (or the mean intensities) of the individual puncta were significantly increased in DK neurons (Fig. 9G, WT = 0.4 ± 0.02 μm^2, DK = 0.8 ± 0.04 μm^2, $P < 0.001$). Furthermore, while most of the synapses (i.e., synaptophysin puncta colocalized with GluR2/3) in WT neurons were found on the dendritic spine (spine synapse, 84.0% ± 2.4%; shaft synapse, 14.9% ± 1.6%), a greater proportion of the DK synapses were formed on the dendritic shaft (spine synapse, 43.7% ± 1.5%; shaft synapse, 56.3% ± 1.5%) (Fig. 9H). Together, these morphological data indicated that while the total number of synapses is reduced, the size of individual synapses is increased in the DK mice. To confirm that the functionality of individual synapses was also enhanced, we analyzed miniature EPSCs (mEPSCs) of hippocampal CA1 neurons and found that both the frequency and amplitude of mEPSCs were significantly higher in the DK slices than in the

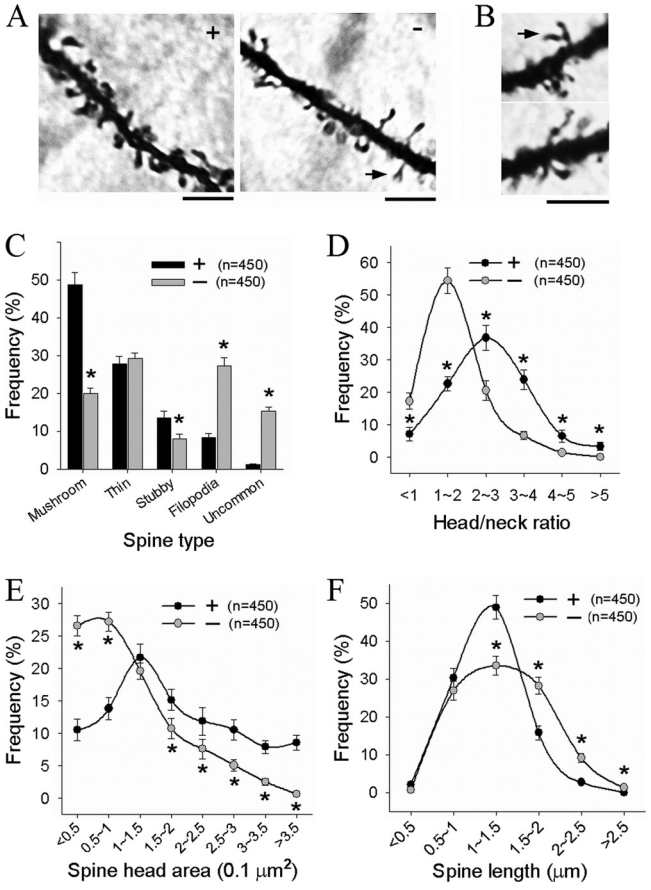

FIG. 8. Abnormal spine morphology in PAK1/PAK3 DK mice. (A, B) Dendritic segments of CA1 neurons with Golgi impregnation showing changes in spine morphology and presence of uncommon spines with spine head branches/protrusions (arrows) in the DK mice. Scale bars, 4 μm. (C to F) Summary graphs showing reduced mushroom spines with increased filopodia and uncommon spines (C), reduced head/neck rations (D), reduced spine head size, and increased spine length (F) in the DK mice. n = number of spines from three animals per genotype.

WT slices (frequency, WT = 0.17 ± 0.02 Hz, DK = 0.26 ± 0.01 Hz, $P < 0.001$; amplitude, WT = 12.85 ± 0.32 pA, DK = 15.06 ± 0.71 pA, $P < 0.01$), suggesting that both transmitter release and postsynaptic responses are elevated in the DK mice. A change in presynaptic function in the DK mice is also supported by decreased paired pulse facilitation in the DK slices (data not shown). Taken together, these results indicate that reduced neuronal complexity has profound effects on synapse development and function, with reduced synapse number but enhanced potency of individual synapses.

Enhanced cofilin activity and perturbed actin network. Finally, to elucidate the molecular mechanisms underlying the structural and functional deficits in PAK1/PAK3 DK mice, we analyzed a number of proteins that might be affected by PAK1 and PAK3. Western blot analysis of protein lysates from whole brain as well as from isolated brain areas (e.g., hippocampus or cortex) showed that despite brain volume reduction, the total protein level of the tested molecules showed no significant alterations in the DK mice (Fig. 10A). However, the basal level of phosphorylated (inactive) cofilin (p-cofilin) was markedly reduced (p-cofilin/cofilin, DK = 23.5% ± 3.3% of WT, $P < 0.0001$ compared to WT; total cofilin, DK = 98.5% ± 2.1% of WT), suggesting that cofilin activity is enhanced in the DK brain. It is important to stress that neither the basal level of p-cofilin nor total cofilin was altered in PAK1 or PAK3 single-KO mice (7, 39), indicating that PAK1 and PAK3 are functionally redundant in regulating cofilin phosphorylation in the brain. Immunohistochemical staining of brain sections also showed that the level of p-cofilin, but not the level of the total protein, was significantly reduced throughout the DK brain (Fig. 10B). It is interesting to note that cofilin expression in the WT animals was detectable throughout the brain but particularly enriched in white matter regions (Fig. 10B, arrowheads), whose volume reductions were particularly striking in the DK brains (Fig. 1). Consistent with enhanced cofilin activity, the amount of F-actin was significantly reduced (CA1 phalloidin intensity, WT = 100% ± 1.6%, DK = 69.7% ± 1.7%, $P < 0.0001$) (Fig. 10C). In cultured hippocampal neurons, F-actin intensity was much higher in actively growing processes in young neurons (day 7) and in the dendritic spines of mature neurons (day 21) than in the adjacent dendritic shaft, whereas in DK neurons, the spine and shaft F-actin intensities were similar (Fig. 10D and E). Moreover, abnormal clusters of F-actin were frequently observed along DK dendrites (Fig. 10D, arrowheads). These results indicate that PAK1 and PAK3 are essential for proper cofilin-mediated F-actin distribution in neuronal processes and suggest that enhanced cofilin activity may contribute to the neuronal deficits in the DK mice. To test this possibility, we treated the DK neurons with a short cell-permeable peptide, pS3. This phosphopeptide is derived from the N-terminal sequence of cofilin containing the phosphorylation site (serine 3) and has been shown to reduce cofilin activity by blocking cofilin phosphatases (1, 62). As shown in Fig. 10F and G, pS3 treatment (40 μg/ml, 2 h) significantly reduced the spine length of the DK neurons compared to the control peptide treatment (control = 3.42 ± 0.09 μm, pS3 = 2.63 ± 0.04 μm, $P < 0.001$). pS3 had no significant effects on the spine length in WT neurons. These results argue that enhanced cofilin function contributes to the spine deficits in the DK mice.

DISCUSSION

Postnatal brain growth in mammals is critical for attaining normal brain size and function, but the underlying mechanisms are poorly understood. In this study, we provide multiple lines of evidence indicating that neuronal size and complexity regulated by PAK1/PAK3-dependent actin cytoskeleton is a key factor responsible for postnatal brain growth and normal brain size. Reduced neuronal complexity has severe effects on synaptic properties, which may underlie the cognitive deficits associated with the DK mice.

It is well documented that human microcephaly is associated with mental retardation and other psychiatric and neurological deficits. However, the relationship between brain size and its cognitive significance in mice is difficult to interpret, because the reduced brain size in mice is often accompanied by abnormalities in gross brain structures, total neuronal loss, and/or altered cellular organization (16, 40, 41, 45). Animal models displaying clearly defined postnatal growth defects but with

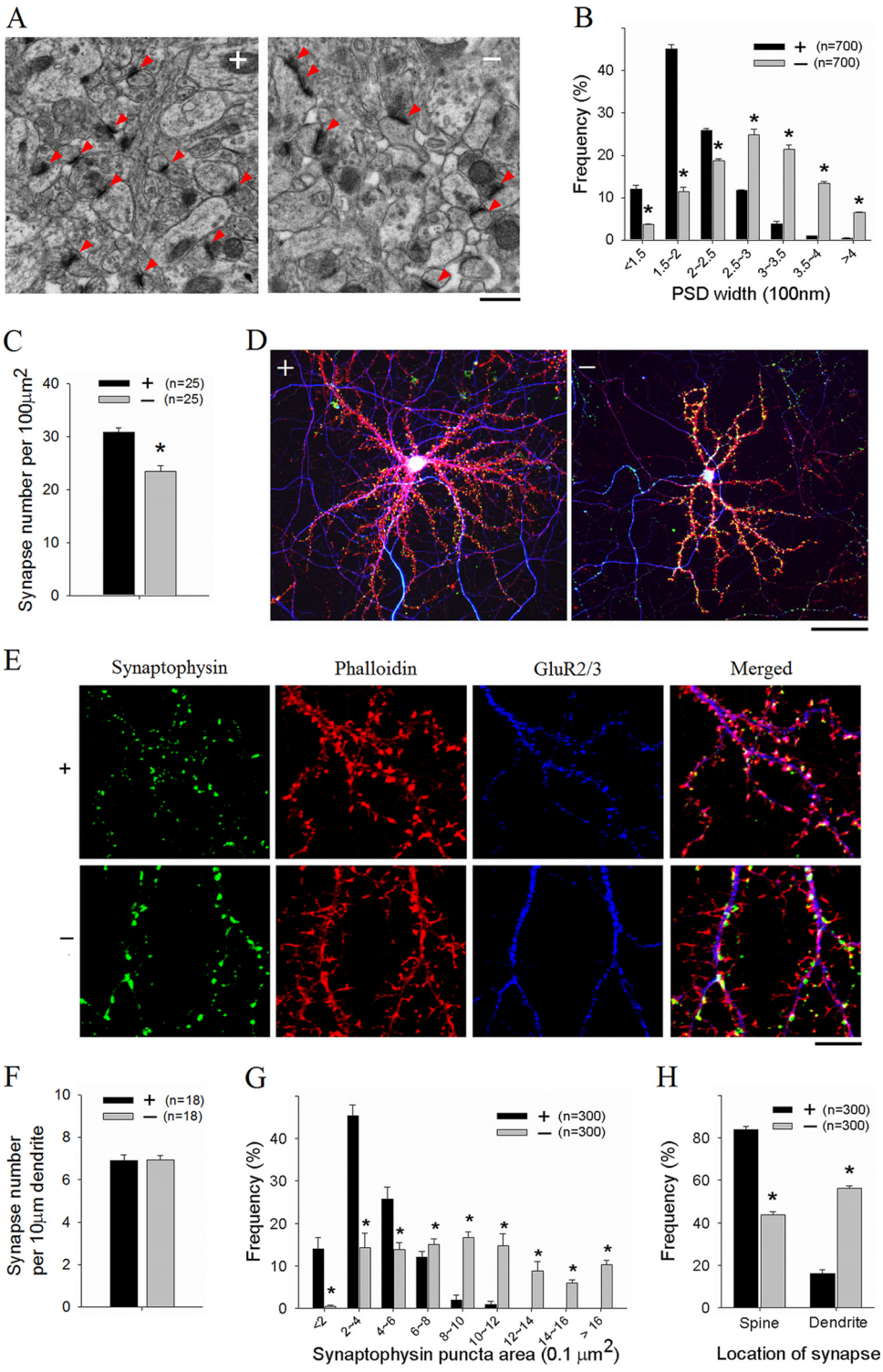

FIG. 9. Reduced synapse density and enlarged individual synapses in PAK1/PAK3 DK mice. (A) EM micrographs of hippocampal CA1 areas showing excitatory synapses (arrowheads). Scale bar, 0.5 μm. (B) Distribution of PSD width (*n* = number of PSDs). (C) Summary graph showing reduction in synapse density in the DK mice (*n* = number of brain sections). (D) Cultured hippocampal neurons triple stained for F-actin (red), pNF (blue), and synaptophsyin (green), showing reduced dendritic (red) and axonal (blue) complexity but enlarged synapses (green) in the DK mice. Scale bar, 50 μm. (E) Triple-stained neurons showing enlarged synaptophysin puncta (green), abnormal spine morphology (phalloidin [red]), abnormal distribution of GluR2/3 (blue), and reduced spine/synaptophysin colocalization in the DK neurons. Scale bar, 10 μm. (F, G, and H) Summary graph of cultured hippocampal neurons showing similar synapse densities per unit of dendrite (G; *n* = number of neurons), larger synaptophysin puncta (G; *n* = number of staining puncta), and decreased spine synapses with increased shaft synapses (H; *n* = number of synapses) in the DK mice.

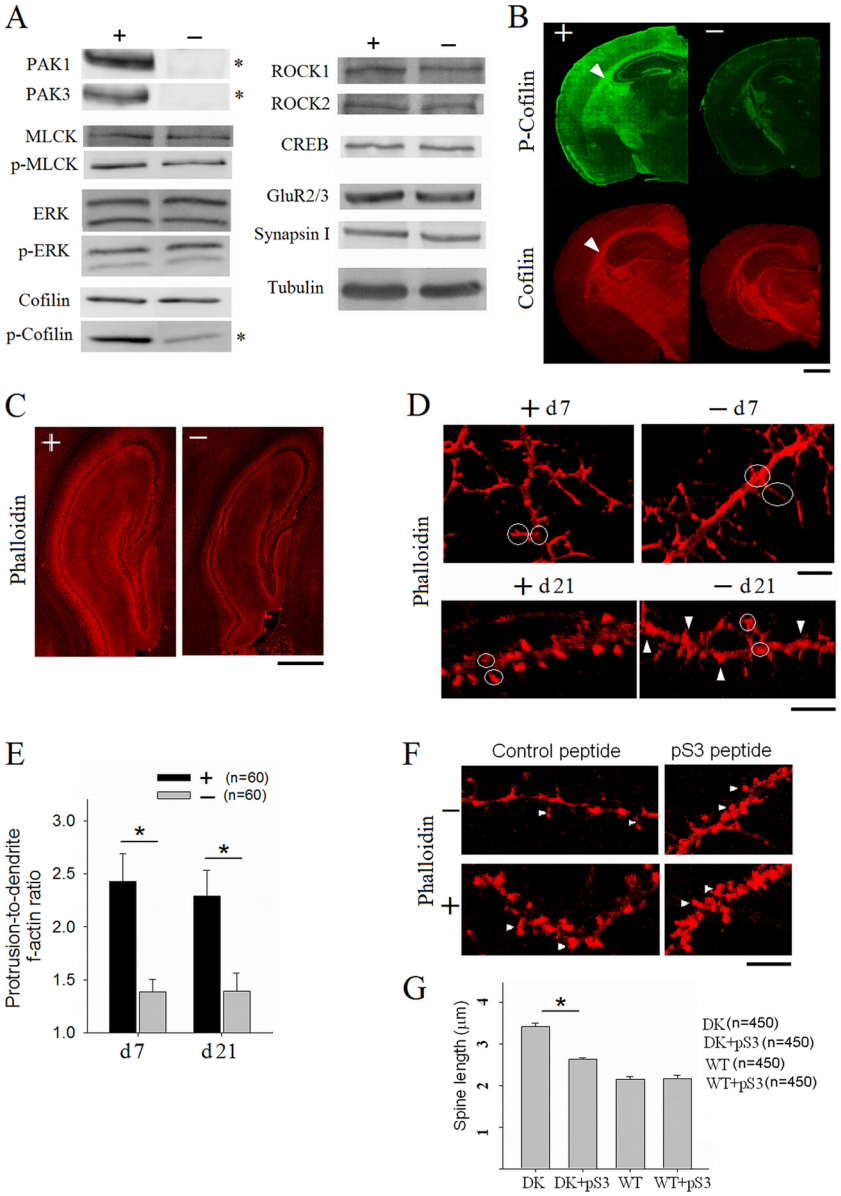

FIG. 10. Increased cofilin activity and reduced F-actin in PAK1/PAK3 DK mice. (A) Western blot showing selective reduction in phosphorylated but not total cofilin in the DK brain. (B) Brain sections stained for cofilin or p-cofilin, showing reduction in p-cofilin but not total cofilin in the DK mice. Scale bar, 1 mm. (C) Hippocampal sections stained for F-actin showing reduction in the amount of F-actin in the DK mice. Scale bar, 0.5 mm. (D) Cultured hippocampal neurons stained for F-actin showing abnormalities in F-actin distribution in both young (day 7) (upper) and mature (day 21) (lower) neurons prepared from DK mice. Circles indicate regions where the F-actin fluorescence intensity ratio was measured (the intensity of growing tips of the dendrites or spines divided by that of adjacent areas). Arrowheads indicate abnormal F-actin clusters. Scale bars, 5 μm. (E) Summary graph showing reduction in the protrusion-to-dendrite F-actin ratio in the DK neurons (n = number of neurons). (F) Cultured hippocampal neurons (day 21) stained for F-actin, showing reduced spine length in pS3-treated (40 μg/ml, 2 h) compared to control peptide-treated DK neurons. Arrows indicate dendritic spines. Scale bar, 5 μm. (G) Summary graph showing reduction in the spine length in pS3-treated compared to control peptide-treated DK neurons but not in WT neurons (n = number of spines).

normal structure and neuronal organization are rare. One such mouse model might be the genetically altered mice lacking the expression of the Rett syndrome gene MECP2 (6, 14, 22). However, these mutant mice display complex neurological symptoms, which ultimately result in death. In addition, the brain size reduction in MECP2 mutant mice is small (−10 to 15%) and is not specific to the brain, because the overall body weight is also reduced. In contrast, the PAK1/PAK3 DK mice display (i) a dramatic and specific postnatal reduction in brain size, (ii) an early defect that coincides with rapid postnatal brain enlargement, (iii) a normal life span and viability without neurological defects, and (iv) a normal brain anatomy and cellular organization. These features make PAK1/PAK3 DK mice a unique and robust model for studying postnatal brain enlargement and its relation to cognition. Accordingly, we show that the DK mice are severely affected in a number of

behaviors, including learning and memory, indicating the critical importance of normal brain size in proper brain function.

A considerable amount of work has been done in both humans and animals to investigate the cellular and molecular mechanisms underlying embryonic brain development. It is now well accepted that generation and migration of the neurons are the primary mechanisms responsible for prenatal brain growth (8, 41, 45), and many molecules involved in these processes have been identified. Notably, these include microcephalin (MCPH1), cyclin-dependent kinase 5 regulatory-associated protein 2 (CDK5RAP2), centromere-associated protein J (CENPJ), and abnormal spindle-like microcephaly-associated protein (ASPM), whose genetic defects are linked to human primary microcephaly and cortical malformations (16, 41). In contrast, relatively few studies have been devoted to postnatal brain enlargement. The results of the present study provide important insights in this respect. In PAK1/PAK3 DK mice, despite a marked reduction (−38%) in brain volume/weight, the change in the total brain cell number is minimal (−10%), indicating that the number of cells is not sufficient for normal postnatal brain growth. However, neuronal dendrites and axons are severely reduced in the DK mice. Importantly, neither the number nor the morphology of glial cells is affected in these mice. These results strongly argue that neuronal complexity is a key determinant of postnatal brain growth and attainment of normal brain volume.

The present study also provides a molecular basis for postnatal brain growth and secondary microcephaly. A number of previous studies have shown that molecules involved in metabolic diseases are associated with secondary microcephaly, but the defects are not specific to the brain, and the reduced brain growth is thought to be caused by insufficient energy supply due to the metabolic defects (e.g., see reference 49). Similarly, although MEPC2 mutant mice show a mild secondary microcephaly phenotype, exactly how this transcription regulator affects postnatal growth remains unknown. Therefore, the present study demonstrating that PAK1/PAK3-dependent signaling is specifically required for *in vivo* neuronal growth and postnatal brain enlargement is of particular importance because it provides a concrete molecular mechanism. In PAK1/PAK3 DK mice, cofilin phosphorylation is reduced, and blocking cofilin activity rescues their spine deficits, suggesting that cofilin-dependent actin regulation may mediate the effect of PAK1/PAK3. However, it is unlikely that cofilin is the only mediator of PAK1/PAK3 action, and further experiments are needed to identify other potential targets. Since PAKs are common downstream substrates of a number of signaling pathways, including those mediated by the Rho/Ras GTPases, neurotrophins, and glutamate receptors (11, 34, 56, 60), and many molecules involved in these pathways have been shown to be important for activity-dependent neuronal morphogenesis *in vitro* (54), it is possible that the PAK1/PAK3-dependent actin reorganization may represent a converged mechanism by which these signaling molecules regulate brain development.

The present study indicates that proper neuronal complexity is critical for establishing normal synaptic connections and functionality in the brain. In PAK1/PAK3 DK mice, although synaptic connections are made, they are clearly different in both structure and function. The increased PSD length in the DK mice appears to be inconsistent with the reduction in the number of mushroom-shaped spines, which normally have a large PSD. One possible interpretation is that more synapses are formed on the dendritic shaft or along the neck of the spine in the DK mice. Another possibility is that although the spine heads are smaller in the DK mice, their PSD occupies a relatively larger proportion of the spine head area compared to the WT mice. Therefore, the PSD size does not necessarily correlate positively with the size of the spine head. Although the PSD enlargement may account for enhanced synaptic responses in the DK mice, other neuronal alterations, including increased membrane resistance, may also contribute to the functional enhancement. In addition to basal synaptic changes, the impairments in long-lasting synaptic plasticity are also prominent in the DK mice. The mechanisms responsible for the reduced bidirectional synaptic plasticity are not clear but may be related to the altered basal synaptic properties and reduced neuronal complexity. Although PAK1/PAK3 may function at mature synapses to directly regulate synaptic plasticity, this is not likely the main reason to account for altered synaptic properties in the DK mice; manipulations of PAKs in adult animals (i.e., without altering neuronal dendrites/axons or brain size) produce no effects on basal synaptic strength and much milder effects on synaptic plasticity and behavioral responses (9, 10, 24). Therefore, we conclude that PAK1 and PAK3 control synaptic properties mainly through balancing the development of proper neuronal complexity/size and individual synaptic potency. In cultured neurons, dendritic complexity regulated by catenins, potent regulators of actin dynamics, has been shown to be inversely correlated with mEPSC amplitudes (47). Thus, coordinated changes in dendritic morphology and unitary excitatory synaptic strength appear to be common mechanisms important for establishing a proper neural circuit both *in vivo* and *in vitro*.

In summary, our analysis of PAK1/PAK3 DK mice has provided the first *in vivo* evidence for PAKs mediating signaling in coordinating neuronal complexity, synaptic properties, and postnatal brain enlargement. Reduced brain size due to simplified neuronal dendrites/axons has severe effects on synapse development and function, which may underlie the behavioral and cognitive deficits associated with microcephalic patients.

ACKNOWLEDGMENTS

This work was supported by grants from the Canadian Institutes of Health Research (CIHR MOP-42396) (Z.J.), Ontario Mental Health Foundation (Z.J.), and the National Basic Research Program (China, 973 Program, 2005CB522501) (W.X.). Wayne Huang was supported by studentships from NSERC and the Hospital for Sick Children research training center.

We are grateful to Cindy Chiang, Alex Han, Christine Laliberté, Matthijs van Eede, and members of the Jia laboratory for technical assistance and comments on the manuscript. The PAK2 and PAK3 cDNA plasmids were kindly provided by Jonathan Chernoff, David Rubinsztein, and Jean-Vianney Barnier.

REFERENCES

1. **Aizawa, H., et al.** 2001. Phosphorylation of cofilin by LIM kinase is necessary for semaphorin 3A-induced growth cone collapse. Nat. Neurosci. **4:**367–373.
2. **Allen, J. D., et al.** 2009. p21-activated kinase regulates mast cell degranulation via effects on calcium mobilization and cytoskeletal dynamics. Blood **113:**2695–2705.
3. **Allen, K. M., et al.** 1998. PAK3 mutation in nonsyndromic X-linked mental retardation. Nat. Genet. **20:**25–30.
4. **Ang, L., J. Kim, V. Stepensky, and H. Hing.** 2003. Dock and Pak regulate olfactory axon pathfinding in Drosophila. Development **130:**1307–1316.

5. **Arias-Romero, L. E., and J. Chernoff.** 2008. A tale of two Paks. Biol. Cell **100:**97–108.
6. **Armstrong, D. D.** 2002. Neuropathology of Rett syndrome. Ment. Retard. Dev. Disabil. Res. Rev. **8:**72–76.
7. **Asrar, S., Y. Meng, Z. Zhou, Z. Todorovski, W. W. Huang, and Z. Jia.** 2009. Regulation of hippocampal long-term potentiation by p21-activated protein kinase 1 (PAK1). Neuropharmacology **56:**73–80.
8. **Ayala, R., T. Shu, and L. H. Tsai.** 2007. Trekking across the brain: the journey of neuronal migration. Cell **128:**29–43.
9. **Boda, B., et al.** 2004. The mental retardation protein PAK3 contributes to synapse formation and plasticity in hippocampus. J. Neurosci. **24:**10816–10825.
10. **Boda, B., L. Jourdain, and D. Muller.** 2008. Distinct, but compensatory roles of PAK1 and PAK3 in spine morphogenesis. Hippocampus **18:**857–861.
11. **Bokoch, G. M.** 2003. Biology of p21-activated kinases. Annu. Rev. Biochem. **72:**743–781.
12. **Cahana, A., et al.** 2001. Targeted mutagenesis of Lis1 disrupts cortical development and LIS1 homodimerization. Proc. Natl. Acad. Sci. U. S. A. **98:**6429–6434.
13. **Causeret, F., et al.** 2009. The p21-activated kinase is required for neuronal migration in the cerebral cortex. Cereb. Cortex **19:**861–875.
14. **Chen, R. Z., S. Akbarian, M. Tudor, and R. Jaenisch.** 2001. Deficiency of methyl-CpG binding protein-2 in CNS neurons results in a Rett-like phenotype in mice. Nat. Genet. **27:**327–331.
15. **Cobos, I., U. Borello, and J. L. R. Rubenstein.** 2007. Dlx transcription factors promote migration through repression of axon and dendrite growth. Neuron **54:**873–888.
16. **Cox, J., A. P. Jackson, J. Bond, and C. G. Woods.** 2006. What primary microcephaly can tell us about brain growth. Trends Mol. Med. **12:**358–366.
17. **Daniels, R. H., P. S. Hall, and G. M. Bokoch.** 1998. Membrane targeting of p21-activated kinase 1 (PAK1) induces neurite outgrowth from PC12 cells. EMBO J. **17:**754–764.
18. **Depaepe, V., et al.** 2005. Ephrin signalling controls brain size by regulating apoptosis of neural progenitors. Nature **435:**1244–1250.
19. **Dorr, A. E., J. P. Lerch, S. Spring, N. Kabani, and R. M. Henkelman.** 2008. High resolution three-dimensional brain atlas using an average magnetic resonance image of 40 adult C57Bl/6J mice. Neuroimage **42:**60–69.
20. **Fan, X., J. P. Labrador, H. Hing, and G. J. Bashaw.** 2003. Slit stimulation recruits Dock and Pak to the roundabout receptor and increases Rac activity to regulate axon repulsion at the CNS midline. Neuron **40:**113–127.
21. **Feng, Y., and C. A. Walsh.** 2004. Mitotic spindle regulation by NdeI controls cerebral cortical size. Neuron **44:**279–293.
22. **Guy, J., B. Hendrich, M. Holmes, J. E. Martin, and A. Bird.** 2001. A mouse Mecp2-null mutation causes neurological symptoms that mimic Rett syndrome. Nat. Genet. **27:**322–326.
23. **Hayashi, K., T. Ohshima, and K. Mikoshiba.** 2002. Pak1 is involved in dendrite initiation as a downstream effector of Rac1 in cortical neurons. Mol. Cell. Neurosci. **20:**579–594.
24. **Hayashi, M. L., et al.** 2004. Altered cortical synaptic morphology and impaired memory consolidation in forebrain-specific dominant-negative PAK transgenic mice. Neuron **42:**773–787.
25. **Hayashi, K., T. Ohshima, M. Hashimoto, and K. Mikoshiba.** 2007. Pak1 regulates dendritic branching and spine formation. Dev. Neurobiol. **67:**655–669.
26. **Hing, H., J. Xiao, N. Harden, L. Lim, and S. L. Zipursky.** 1999. Pak functions downstream of Dock to regulate photoreceptor axon guidance in Drosophila. Cell **97:**853–863.
27. **Hirotsune, S., et al.** 1998. Graded reduction of Pafah1b1 (Lis1) activity results in neuronal migration defects and early embryonic lethality. Nat. Genet. **19:**333–339.
28. **Hu, H., T. F. Marton, and C. S. Goodman.** 2001. Plexin B mediates axon guidance in Drosophila by simultaneously inhibiting active Rac and enhancing RhoA signaling. Neuron **32:**39–51.
29. **Jacobs, T., et al.** 2007. Localized activation of p21-activated kinase controls neuronal polarity and morphology. J. Neurosci. **27:**8604–8615.
30. **Kreis, P., E. Thévenot, V. Rousseau, B. Boda, D. Muller, and J. V. Barnier.** 2007. The p21-activated kinase 3 implicated in mental retardation regulates spine morphogenesis through a Cdc42-dependent pathway. J. Biol. Chem. **282:**21497–21506.
31. **Kreis, P., and J. Barnier.** 2009. PAK signalling in neuronal physiology. Cell. Signal. **21:**384–393.
32. **Li, X., and A. Minden.** 2003. Targeted disruption of the gene for the PAK5 kinase in mice. Mol. Cell. Biol. **23:**7134–7142.
33. **Lucanic, M., M. Kiley, N. Ashcroft, N. L'etoile, and H. Cheng.** 2006. The Caenorhabditis elegans p21-activated kinases are differentially required for UNC-6/netrin-mediated commissural motor axon guidance. Development **133:**4549–4559.
34. **Luo, L.** 2000. Rho GTPases in neuronal morphogenesis. Nat. Rev. Neurosci. **1:**173–180.
35. **Malenka, R. C., and M. F. Bear.** 2004. LTP and LTD: an embarrassment of riches. Neuron **44:**5–21.
36. **Marler, K. J. M., R. Kozma, S. Ahmed, J. Dong, C. Hall, and L. Lim.** 2005. Outgrowth of neurites from NIE-115 neuroblastoma cells is prevented on repulsive substrates through the action of PAK. Mol. Cell. Biol. **25:**5226–5241.
37. **McPhie, D. L., et al.** 2003. DNA synthesis and neuronal apoptosis caused by familial Alzheimer disease mutants of the amyloid precursor protein are mediated by the p21 activated kinase PAK3. J. Neurosci. **23:**6914–6927.
38. **Meng, Y., et al.** 2002. Abnormal spine morphology and enhanced LTP in LIMK-1 knockout mice. Neuron **35:**121–133.
39. **Meng, J., Y. Meng, A. Hanna, C. Janus, and Z. Jia.** 2005. Abnormal long-lasting synaptic plasticity and cognition in mice lacking the mental retardation gene Pak3. J. Neurosci. **25:**6641–6650.
40. **Mochida, G. H., and C. A. Walsh.** 2001. Molecular genetics of human microcephaly. Curr. Opin. Neurol. **14:**151–156.
41. **Mochida, G. H.** 2009. Genetics and biology of microcephaly and lissencephaly. Semin. Pediatr. Neurol. **16:**120–126.
42. **Nekrasova, T., M. L. Jobes, J. H. Ting, G. C. Wagner, and A. Minden.** 2008. Targeted disruption of the Pak5 and Pak6 genes in mice leads to deficits in learning and locomotion. Dev. Biol. **322:**95–108.
43. **Nikolić, M.** 2008. The Pak1 kinase: an important regulator of neuronal morphology and function in the developing forebrain. Mol. Neurobiol. **37:**187–202.
44. **Ong, W. Y., X. S. Wang, and E. Manser.** 2002. Differential distribution of alpha and beta isoforms of p21-activated kinase in the monkey cerebral neocortex and hippocampus. Exp. Brain Res. **144:**189–199.
45. **Pang, T., R. Atefy, and V. Sheen.** 2008. Malformations of cortical development. Neurologist **14:**181–191.
46. **Peippo, M., A. M. Koivisto, T. Särkämö, M. Sipponen, H. von Koskull, T. Ylisaukko-oja, K. Rehnström, G. Froyen, J. Ignatius, and I. Järvelä.** 2007. PAK3 related mental disability: further characterization of the phenotype. Am. J. Med. Genet. A **143A:**2406–2416.
47. **Peng, Y. R., et al.** 2009. Coordinated changes in dendritic arborization and synaptic strength during neural circuit development. Neuron **61:**71–84.
48. **Qu, J., et al.** 2003. PAK4 kinase is essential for embryonic viability and for proper neuronal development. Mol. Cell. Biol. **23:**7122–7133.
49. **Rosenberg, M. J., et al.** 2002. Mutant deoxynucleotide carrier is associated with congenital microcephaly. Nat. Genet. **32:**175–179.
50. **Sakakibara, A., and A. F. Horwitz.** 2006. Mechanism of polarized protrusion formation on neuronal precursors migrating in the developing chicken cerebellum. J. Cell Sci. **119:**3583–3592.
51. **Sandig, V., et al.** 2000. Optimization of the helper-dependent adenovirus system for production and potency in vivo. Proc. Natl. Acad. Sci. U. S. A. **97:**1002–1007.
52. **Silver, D. L., et al.** 2010. The exon junction complex component Magoh controls brain size by regulating neural stem cell division. Nat. Neurosci. **13:**551–558.
53. **Souopgui, J., M. Sölter, and T. Pieler.** 2002. XPak3 promotes cell cycle withdrawal during primary neurogenesis in Xenopus laevis. EMBO J. **21:**6429–6439.
54. **Urbanska, M., M. Blazejczyk, and J. Jaworski.** 2008. Molecular basis of dendritic arborization. Acta Neurobiol. Exp. **68:**264–288.
55. **Vadlamudi, R. K., B. Manavathi, R. R. Singh, D. Nguyen, F. Li, and R. Kumar.** 2005. An essential role of Pak1 phosphorylation of SHARP in Notch signaling. Oncogene **24:**4591–4596.
56. **van Galen, E. J., and G. J. Ramakers.** 2005. Rho proteins, mental retardation and the neurobiological basis of intelligence. Prog. Brain Res. **147:**295–317.
57. **Walf, A. A., and C. A. Frye.** 2007. The use of the elevated plus maze as an assay of anxiety-related behavior in rodents. Nat. Protoc. **2:**322–328.
58. **Woods, C. G.** 2004. Human microcephaly. Curr. Opin. Neurobiol. **14:**112–117.
59. **Zhang, H., D. J. Webb, H. Asmussen, S. Niu, and A. F. Horwitz.** 2005. A GIT1/PIX/Rac/PAK signaling module regulates spine morphogenesis and synapse formation through MLC. J. Neurosci. **25:**3379–3388.
60. **Zhao, Z. S., and E. Manser.** 2005. PAK and other Rho-associated kinases—effectors with surprisingly diverse mechanisms of regulation. Biochem. J. **386:**201–214.
61. **Zhong, J. L., M. D. Banerjee, and M. Nikolic.** 2003. Pak1 and its T212 phosphorylated form accumulate in neurones and epithelial cells of the developing rodent. Dev. Dyn. **228:**121–127.
62. **Zhou, Q., K. J. Homma, and M. M. Poo.** 2004. Shrinkage of dendritic spines associated with long-term depression of hippocampal synapses. Neuron **44:**749–757.